

Rapid assessment of SARS-CoV-2 evolved variants using virus-like particles

Abdullah M. Syed^{1,2†}, Taha Y. Taha^{3†}, Takako Tabata^{3†}, Irene P. Chen^{3,4}, Alison Ciling², Mir M. Khalid³, Bharath Sreekumar³, Pei-Yi Chen³, Jennifer M. Hayashi³, Katarzyna M. Soczek^{2,5}, Melanie Ott^{2,3,6*}, Jennifer A. Doudna^{1,2,5,7,8,9,10*}

¹Gladstone Institute of Data Science and Biotechnology, San Francisco, CA, USA. ²Innovative Genomics Institute, University of California, Berkeley, Berkeley, CA, USA. ³Gladstone Institute of Virology, San Francisco, CA, USA. ⁴Biomedical Sciences Graduate Program, University of California, San Francisco, CA, USA. ⁵Department of Molecular and Cell Biology, University of California, Berkeley, CA, USA. ⁶Department of Medicine, University of California San Francisco, CA, USA. ⁷Molecular Biophysics and Integrated Bioimaging Division, Lawrence Berkeley National Laboratory, Berkeley, CA, USA. ⁸Howard Hughes Medical Institute, University of California, Berkeley, Berkeley, CA, USA. ⁹Department of Chemistry, University of California, Berkeley, Berkeley, CA, USA. ¹⁰California Institute for Quantitative Biosciences (QB3), University of California, Berkeley, Berkeley, CA, USA.

†These authors contributed equally to this work.

*Corresponding author. Email: doudna@berkeley.edu (J.A.D.); melanie.ott@gladstone.ucsf.edu (M.O.)

Efforts to determine why new SARS-CoV-2 variants demonstrate improved fitness have been limited to analyzing mutations in the spike (S) protein using S-pseudotyped particles. Here we show that SARS-CoV-2 virus-like particles (SC2-VLPs) can package and deliver exogenous transcripts, enabling analysis of mutations within all structural proteins and at multiple steps in the viral life cycle. In SC2-VLPs, four nucleocapsid (N) mutations found universally in more-transmissible variants independently increased mRNA delivery and expression by ~10-fold, and in a reverse genetics model, S202R and R203M each produced >50-fold more virus. SC2-VLPs provide a platform for rapid testing of viral variants outside a biosafety level 3 setting and demonstrate N mutations and particle assembly to be mechanisms that could explain the increased spread of variants, including Delta (R203M).

The COVID-19 pandemic is a leading cause of death globally due to the ongoing emergence of SARS-CoV-2 variants with increased transmissibility. Understanding the molecular determinants of enhanced infectivity is central to vaccine and therapeutic development, but research is hindered because SARS-CoV-2 can only be studied in a biosafety level 3 (BSL-3) lab. Furthermore, generating mutant infectious clones of SARS-CoV-2 is technically challenging (1–5). Current studies employ spike (S) pseudotyped lentivirus systems for evaluation of S-mediated ACE2 receptor binding and cell entry (6, 7). However, most mutations in circulating variants occur outside the S gene and are thus inaccessible by this approach (8).

All SARS-CoV-2 variants of interest or concern defined by the WHO contain at least one mutation with >50% penetrance within seven amino acids (N:199–205) in the nucleocapsid (N) protein, which is required for replication and RNA binding, packaging, stabilization and release (8). Despite its functional importance and emergence as a mutational hotspot, the N protein has not been widely studied because of the absence of simple and safe cell-based assays. Biochemical analysis of N has also proven difficult because of its instability and propensity to assemble or phase-separate and to bind RNA non-specifically (9–11). To investigate N function, effects of mutations and other aspects of SARS-CoV-2

biology, we set out to develop a system to package and deliver exogenous RNA transcripts into cells using virus-like particles (VLPs).

We reasoned that a process mimicking viral assembly to package and deliver reporter transcripts would simplify the analysis of successful virus production, budding and entry. Previous studies have shown that co-expression of only the structural proteins of coronaviruses generates VLPs containing all four structural proteins (12–17). These VLPs appear to have similar morphology to infectious viruses and have been proposed as vaccine candidates (18). A key requirement for such VLPs to deliver reporter transcripts into cells is the recognition of a cis-acting RNA sequence that triggers packaging. During viral assembly, the N protein is thought to recognize one or more RNA structures within ORF1ab, enabling the full viral genome that contains this sequence to be packaged to the exclusion of viral subgenomic and host transcripts (19). The identification of such a SARS-CoV-2 cis-acting RNA element is required to create SARS-CoV-2 VLPs (SC2-VLPs) that incorporate and deliver engineered transcripts by this mechanism.

Based on the reported packaging sequences for related viruses, including Murine Hepatitis Virus and SARS-CoV-1, we hypothesized that the SARS-CoV-2 packaging signal might reside within a region we termed “T20” (nt 20080–22222)

encoding non-structural protein 15 (nsp15) and nsp16 (Fig. 1A) (16, 19–21). We designed a transfer plasmid encoding a luciferase transcript containing T20 within its 3' untranslated region (UTR). We tested for SC2-VLP production by co-transfecting the transfer plasmid into packaging cells (293T) along with plasmids encoding the viral structural proteins (Fig. 1B). Supernatant collected from these cells was filtered and incubated with receiver 293T cells co-expressing SARS-CoV-2 entry factors ACE2 and TMPRSS2 (Fig. 1B). We observed luciferase expression in receiver cells only in the presence of all structural proteins (S, M, N, E) as well as the T20-containing reporter transcript (Fig. 1C). Substituting any one of the structural proteins or the luciferase-T20 transcript with a luciferase-only transcript decreased luminescence in receiver cells by >200-fold and 63-fold, respectively (Fig. 1C). We also conducted this experiment using Vero E6 cells that endogenously express ACE2 and once again observed robust luciferase expression only in the presence of all five components (fig. S1A).

VLP-mediated transcript delivery required untagged native M protein and a low ratio of S expression plasmid relative to the other plasmids (Fig. 1, D and E, and fig. S1B). This is expected since S is expressed at lower levels compared to other structural proteins during infection (22). SC2-VLPs should also require lower S expression compared to pseudovirus systems because S assembles along with the other structural proteins within the ER-Golgi intermediate compartment, while pseudovirus assays typically require accumulation of S at the plasma membrane followed by random incorporation into budding particles (23, 24). Interestingly, we detected N and S proteins within pelleted material (Fig. 1, F and G) from multiple conditions that did not yield luciferase expression in receiver cells, suggesting that particles produced under less stringent conditions are not competent for delivering mRNA. These findings suggest that co-expression of structural proteins likely produces VLPs as well as defective particles, and mRNA delivery requires more stringent conditions.

Further analysis showed that SC2-VLPs are stable against ribonuclease A, resistant to freeze-thaw treatment (fig. S2A), can be concentrated by precipitation, ultrafiltration and ultracentrifugation (fig. S2B) and induce transient expression of luciferase (fig. S2C). Analysis of SC2-VLPs by sucrose gradient ultracentrifugation showed that large dense particles are responsible for inducing luciferase expression (Fig. 1, H and I). These data show that SC2-VLPs are formed under our experimental conditions and deliver selectively packaged transcripts.

Next, we determined the optimal SARS-CoV-2 cis-acting RNA sequence for SC2-VLP mediated delivery. We generated a library of 28 2-kb overlapping tiled segments (numbered T1-T28, table S1) from the SARS-CoV-2 genome and inserted

them individually into a luciferase-encoding plasmid (Fig. 2A). SC2-VLPs generated using luciferase-encoding plasmids that included any region of ORF1ab produced detectable luminescence, suggesting that SARS-CoV-2 packaging may not rely entirely on one contiguous cis-acting RNA element (Fig. 2, B and C). Furthermore, luciferase-encoding plasmids that included fragments T24-28 resulted in lower luciferase expression (Fig. 2, B and C), consistent with the exclusion of subgenomic viral transcripts containing these sequences to minimize production of replication-defective virus particles. Overall, luciferase expression was most efficient using T20 (nt 20080 - 22222) located near the 3' end of ORF1ab (Fig. 2, B and C) and partially but not completely overlapping with PS580 (19785-20348), which was previously predicted to be the packaging signal for SARS-CoV-1 based on structural similarity to known coronavirus packaging signals (16).

To further define the minimal cis-acting RNA element sufficient for SC2-VLP mediated delivery, we tested truncations and additions to T20 as well as PS580 from SARS-CoV-1. We found that PS580 resulted in lower luciferase expression compared to T20 (Fig. 2, D and E, and fig. S3, A and B). We observed the highest luciferase expression level from SC2-VLPs encoding the nucleotide sequence 20080-21171 (termed PS9), and further truncations of this sequence reduced expression (Fig. 2, D and E, and fig. S3, A and B). We used PS9 to generate VLPs encoding GFP and found that they induced GFP expression in receiver cells (Fig. 2F). These data suggest that PS9 (nt 20080-21171) is a cis-acting element that is sufficient for triggering RNA packaging into SC2-VLPs although it is not currently known whether this sequence is required for the packaging of the SARS-CoV-2 genome.

SC2-VLPs provide a new and more physiological model compared to pseudoviruses for testing mutations in all viral structural proteins (S, E, M, N) for effects on assembly, packaging and cell entry. Surprisingly, none of the 15 SC2-VLPs generated with S mutant genes, including four with the combined mutations found in the Alpha, Beta, Gamma and Epsilon variants, increased luciferase expression in transduced cells beyond that observed for the original SC2-VLPs (Fig. 3, A and B, and table S2). Since nearly all circulating variants contain the S:D614G mutation, we compared all mutants to the ancestral S protein modified to include G614 (termed WT+D614G). Minor changes in S expression between mutants may be a confounding factor since SC2-VLPs mediate luciferase expression optimally in a narrow range of S expression. Over a range of 6.25 ng to 50 pg per well of S-encoding plasmid, none of the tested S mutations produced >2-fold improvement in luciferase expression (fig. S4, A and B); slightly improved luciferase expression occurred with the S sequence derived from the Alpha variant (B.1.1.7) and S containing the mutation N501Y within the receptor binding domain. These findings contrast with prior results using S-pseudotyped

lentiviruses, where enhanced entry was reported for some S mutations including S:N501Y (25, 26). However, S mutations tested in the context of SARS-CoV-2 infectious clones have shown mixed effects, and mutations within S may also mediate enhanced transmission by interfering with the binding of neutralizing antibodies (27, 28). We tested whether VLPs could also be used to measure antibody neutralization and found results similar to previously reported data using a pseudovirus neutralization assay (Fig. 3C and fig. S4C). Using a neutralizing monoclonal antibody (MM43), we observed dose-dependent inhibition of luminescence with a measured IC₅₀ of 0.35 µg/mL, similar to the manufacturer reported IC₅₀ of 1.41 µg/mL. We also tested S from circulating variants and observed robust MM43-mediated neutralization of SC2-VLPs generated using Alpha, Beta, Gamma, Delta and Epsilon variant S proteins (Fig. 3D) and consistent with previous studies (29). These results show that SC2-VLPs employ S mediated entry and can be used for screening S-mutations for entry and neutralization. Although we did not observe enhanced entry due to the S mutations we tested, these mutations could still provide a fitness advantage for SARS-CoV-2 by limiting antibody mediated neutralization. Detailed characterization of S mutations and their sensitivity to neutralizing antibodies has been examined by other studies (30, 31).

We next tested whether N mutations found in circulating variants improve viral particle assembly, RNA delivery and/or reporter gene expression using SC2-VLPs. We tested 15 N mutations including two combinations corresponding to the Alpha and Gamma variants since they both contain the co-occurring R203K/G204R mutations. The Alpha and Gamma variant N improved luciferase expression in receiver cells by 7.5- and 4.2-fold respectively relative to the ancestral Wuhan Hu-1 N-protein (Fig. 3E). In addition, four single amino acid changes improved luciferase expression: P199L, S202R, R203K and R203M. Two of these mutations do not change the overall charge (P199L, R203K), one results in a more positive charge (S202R), and one results in a more negative charge (R203M), suggesting that the improvement in luciferase expression is not likely due to simple electrostatics. Western blotting revealed no correlation between N protein expression levels and luciferase induction, suggesting that these N mutations enhance luciferase induction through a different mechanism (fig. S5). Interestingly, half of the amino acid changes observed within N and all of the mutations observed to enhance luminescence occur within a seven amino acid region (aa199-205) of the central disordered region (termed the “linker” region, Fig. 3F) suggestive of a shared mechanism.

Further analysis of six N mutants was conducted to determine whether these mutations affect SC2-VLP assembly efficiency, RNA packaging, or RNA uncoating prior to expression. We chose the three mutants that demonstrated ~10-fold

improved luciferase expression (P199L, S202R, R203M) and two mutants that did not increase luciferase expression significantly (G204R, M234I) in the preliminary screen and compared these to the wild type (Fig. 4A). N protein expression levels were similar in packaging cells, except for G204R, and did not correlate with luciferase expression (Fig. 4, A and B). We then purified SC2-VLPs containing each N mutation and found that those containing P199L and S202R had increased levels of S, N and luciferase RNA while R203M showed increased luciferase RNA only (Fig. 4C). These results suggest that mutations within the N linker domain improve the assembly of SC2-VLPs, leading either to greater overall VLP production, a larger fraction of VLPs that contain RNA or higher RNA content per particle. In either case, these results suggest a previously unanticipated explanation for the increased fitness and spread of SARS-CoV-2 variants of concern.

To validate whether the effects we observed in SC2-VLPs improve replication of intact virus, we used reverse genetics to generate SARS-CoV-2 containing N:S202R and N:R203M substitutions within a USA/WA1-2020 (Washington isolate) background (1) (Fig. 4D). We generated and NGS-verified stocks of virus containing the indicated mutations (fig. S6). We infected A549-ACE2 cells with wildtype, N:S202R, or N:R203M at a multiplicity of infection (MOI) of 0.1 and collected supernatants at 24, 48 and 72 hours post infection. RT-qPCR indicated 45-fold and 23-fold higher RNA content in the supernatant at 72 hours post infection, and plaque assays indicated 166-fold and 51-fold higher infectious titers for N:S202R and N:R203M virus, respectively (Fig. 4, E to G). Our results indicate that both of these mutations enhance replication in lung epithelial cells, consistent with our observations using SC2-VLPs.

Overall, we present a strategy for rapidly generating and analyzing SC2-VLPs that package and deliver exogenous mRNA. This approach allows examination of viral assembly, budding, stability, maturation, entry and genome uncoating involving all of the viral structural proteins (S, E, M, N) without generating replication-competent virus. Such a strategy is useful not only for dissecting the molecular virology of SARS-CoV-2 but also for future development and screening of therapeutics targeting assembly, budding, maturation and entry. This strategy is ideally suited for the development of new antivirals targeting SARS-CoV-2 as it is sensitive, quantitative and scalable to high-throughput workflows. The unexpected finding of improved mRNA packaging and luciferase induction by mutations within the N protein points to a previously unknown strategy for coronaviruses to evolve enhanced viral fitness. The mechanism for this enhancement involves increased mRNA packaging and delivery although the exact process is currently unknown. Recent literature suggests that these mutations may affect phosphorylation of N,

its binding to RNA and phase separation behavior all of which could impact the efficiency of assembly (32–34). Our observations of enhanced RNA packaging and replication are consistent with recent reports that the Delta variant (containing N:R203M) generates 1000-fold higher levels of viral RNA within patients (35). Our results provide a molecular basis to explain why the SARS-CoV-2 Delta variant demonstrates improved viral fitness.

REFERENCES AND NOTES

- Xie, A. Muruato, K. G. Lokugamage, K. Narayanan, X. Zhang, J. Zou, J. Liu, C. Schindewolf, N. E. Bopp, P. V. Aguilar, K. S. Plante, S. C. Weaver, S. Makino, J. W. LeDuc, V. D. Menachery, P.-Y. Shi, An Infectious cDNA Clone of SARS-CoV-2. *Cell Host Microbe* **27**, 841–848.e3 (2020). [doi:10.1016/j.chom.2020.04.004](https://doi.org/10.1016/j.chom.2020.04.004) [Medline](#)
- Torii, C. Ono, R. Suzuki, Y. Morioka, I. Anzai, Y. Fauzyah, Y. Maeda, W. Kamitani, T. Fukuhara, Y. Matsuura, Establishment of a reverse genetics system for SARS-CoV-2 using circular polymerase extension reaction. *Cell Rep.* **35**, 109014 (2021). [doi:10.1016/j.celrep.2021.109014](https://doi.org/10.1016/j.celrep.2021.109014) [Medline](#)
- C. Ye, K. Chiem, J.-G. Park, F. Oladunni, R. N. Platt 2nd, T. Anderson, F. Almazan, J. C. de la Torre, L. Martinez-Sobrido, Rescue of SARS-CoV-2 from a Single Bacterial Artificial Chromosome. *mBio* **11**, e02168-20 (2020). [doi:10.1128/mBio.02168-20](https://doi.org/10.1128/mBio.02168-20) [Medline](#)
- X. Xie, K. G. Lokugamage, X. Zhang, M. N. Vu, A. E. Muruato, V. D. Menachery, P.-Y. Shi, Engineering SARS-CoV-2 using a reverse genetic system. *Nat. Protoc.* **16**, 1761–1784 (2021). [doi:10.1038/s41596-021-00491-8](https://doi.org/10.1038/s41596-021-00491-8) [Medline](#)
- S. J. Rihn, A. Merits, S. Bakshi, M. L. Turnbull, A. Wickenhagen, A. J. T. Alexander, C. Baillie, B. Brennan, F. Brown, K. Bruncker, S. R. Bryden, K. A. Burness, S. Carmichael, S. J. Cole, V. M. Cowton, P. Davies, C. Davis, G. De Lorenzo, C. L. Donald, M. Dorward, J. I. Dunlop, M. Elliott, M. Fares, A. da Silva Filipe, J. R. Freitas, W. Furnon, R. J. Gestuveo, A. Geyer, D. Giesel, D. M. Goldfarb, N. Goodman, R. Gunson, C. J. Hastie, V. Herder, J. Hughes, C. Johnson, N. Johnson, A. Kohl, K. Kerr, H. Leech, L. S. Lello, K. Li, G. Lieber, X. Liu, R. Lingala, C. Loney, D. Mair, M. J. McElwee, S. McFarlane, J. Nichols, K. Nomikou, A. Orr, R. J. Orton, M. Palmarini, Y. A. Parr, R. M. Pinto, S. Raggett, E. Reid, D. L. Robertson, J. Royle, N. Cameron-Ruiz, J. G. Shepherd, K. Smollett, D. G. Stewart, M. Stewart, E. Sugrue, A. M. Sziemiel, A. Taggart, E. C. Thomson, L. Tong, L. S. Torrie, R. Toth, M. Varjak, S. Wang, S. G. Wilkinson, P. G. Wyatt, E. Zusinaite, D. R. Alessi, A. H. Patel, A. Zaid, S. J. Wilson, S. Mahalingam, A plasmid DNA-launched SARS-CoV-2 reverse genetics system and coronavirus toolkit for COVID-19 research. *PLoS Biol.* **19**, e3001091 (2021). [doi:10.1371/journal.pbio.3001091](https://doi.org/10.1371/journal.pbio.3001091) [Medline](#)
- J. A. Plante, Y. Liu, J. Liu, H. Xia, B. A. Johnson, K. G. Lokugamage, X. Zhang, A. E. Muruato, J. Zou, C. R. Fontes-Garfias, D. Mirchandani, D. Scharton, J. P. Billelo, Z. Ku, Z. An, B. Kalveram, A. N. Freiberg, V. D. Menachery, X. Xie, K. S. Plante, S. C. Weaver, P.-Y. Shi, Spike mutation D614G alters SARS-CoV-2 fitness. *Nature* **592**, 116–121 (2021). [doi:10.1038/s41586-020-2895-3](https://doi.org/10.1038/s41586-020-2895-3) [Medline](#)
- K. H. D. Crawford, R. Eguia, A. S. Dingens, A. N. Loes, K. D. Malone, C. R. Wolf, H. Y. Chu, M. A. Tortorici, D. Velesler, M. Murphy, D. Pettie, N. P. King, A. B. Balazs, J. D. Bloom, Protocol and Reagents for Pseudotyping Lentiviral Particles with SARS-CoV-2 Spike Protein for Neutralization Assays. *Viruses* **12**, 513 (2020). [doi:10.3390/v12050513](https://doi.org/10.3390/v12050513) [Medline](#)
- A. A. Latif, J. L. Mullen, M. Alkuzweny, G. Tsueng, M. Cano, E. Haag, J. Zhou, M. Zeller, E. Hufbauer, N. Matteson, C. Wu, K. G. Andersen, A. I. Su, K. G. Gangavarapu, L. D. Hughes; the Center for Viral Systems Biology, Lineage comparison. [outbreak.info](https://outbreak.info/compare-lineages) (available at <https://outbreak.info/compare-lineages>), accessed 22 July 2021.
- W. Zeng, G. Liu, H. Ma, D. Zhao, Y. Yang, M. Liu, A. Mohammed, C. Zhao, Y. Yang, J. Xie, C. Ding, X. Ma, J. Weng, Y. Gao, H. He, T. Jin, Biochemical characterization of SARS-CoV-2 nucleocapsid protein. *Biochem. Biophys. Res. Commun.* **527**, 618–623 (2020). [doi:10.1016/j.bbrc.2020.04.136](https://doi.org/10.1016/j.bbrc.2020.04.136) [Medline](#)
- J. Cubuk, J. J. Alston, J. J. Incicco, S. Singh, M. D. Stuchell-Breteron, M. D. Ward, M. I. Zimmerman, N. Vithani, D. Griffith, J. A. Wagoner, G. R. Bowman, K. B. Hall, A. Soranno, A. S. Holehouse, The SARS-CoV-2 nucleocapsid protein is dynamic, disordered, and phase separates with RNA. *Nat. Commun.* **12**, 1936 (2021). [doi:10.1038/s41467-021-21953-3](https://doi.org/10.1038/s41467-021-21953-3) [Medline](#)
- T. M. Perdikari, A. C. Murthy, V. H. Ryan, S. Watters, M. T. Naik, N. L. Fawzi, SARS-CoV-2 nucleocapsid protein phase-separates with RNA and with human hnRNPs. *EMBO J.* **39**, e106478 (2020). [doi:10.15252/embj.2020106478](https://doi.org/10.15252/embj.2020106478) [Medline](#)
- C. B. Plescia, E. A. David, D. Patra, R. Sengupta, S. Amiar, Y. Su, R. V. Stahelin, SARS-CoV-2 viral budding and entry can be modeled using BSL-2 level virus-like particles. *J. Biol. Chem.* **296**, 100103 (2021). [doi:10.1074/jbc.RA120.016148](https://doi.org/10.1074/jbc.RA120.016148) [Medline](#)
- H. Swann, A. Sharma, B. Preece, A. Peterson, C. Eldredge, D. M. Belnap, M. Vershinin, S. Saffarian, Minimal system for assembly of SARS-CoV-2 virus like particles. *Sci. Rep.* **10**, 21877 (2020). [doi:10.1038/s41598-020-78656-w](https://doi.org/10.1038/s41598-020-78656-w) [Medline](#)
- J. Lu, G. Lu, S. Tan, J. Xia, H. Xiong, X. Yu, Q. Qi, X. Yu, L. Li, H. Yu, N. Xia, T. Zhang, Y. Xu, J. Lin, A COVID-19 mRNA vaccine encoding SARS-CoV-2 virus-like particles induces a strong antiviral-like immune response in mice. *Cell Res.* **30**, 936–939 (2020). [doi:10.1038/s41422-020-00392-7](https://doi.org/10.1038/s41422-020-00392-7) [Medline](#)
- Y. L. Siu, K. T. Teoh, J. Lo, C. M. Chan, F. Kien, N. Escricou, S. W. Tsao, J. M. Nicholls, R. Altmeyer, J. S. M. Peiris, R. Bruzzone, B. Nal, The M, E, and N structural proteins of the severe acute respiratory syndrome coronavirus are required for efficient assembly, trafficking, and release of virus-like particles. *J. Virol.* **82**, 11318–11330 (2008). [doi:10.1128/JVI.01052-08](https://doi.org/10.1128/JVI.01052-08) [Medline](#)
- P.-K. Hsieh, S. C. Chang, C.-C. Huang, T.-T. Lee, C.-W. Hsiao, Y.-H. Kou, I.-Y. Chen, C.-K. Chang, T.-H. Huang, M.-F. Chang, Assembly of severe acute respiratory syndrome coronavirus RNA packaging signal into virus-like particles is nucleocapsid dependent. *J. Virol.* **79**, 13848–13855 (2005). [doi:10.1128/JVI.79.22.13848-13855.2005](https://doi.org/10.1128/JVI.79.22.13848-13855.2005) [Medline](#)
- S. Dent, B. W. Neuman, Purification of coronavirus virions for Cryo-EM and proteomic analysis. *Coronaviruses* **1282**, 99–108 (2015). [doi:10.1007/978-1-4939-2438-7_10](https://doi.org/10.1007/978-1-4939-2438-7_10) [Medline](#)
- X. Lu, Y. Chen, B. Bai, H. Hu, L. Tao, J. Yang, J. Chen, Z. Chen, Z. Hu, H. Wang, Immune responses against severe acute respiratory syndrome coronavirus induced by virus-like particles in mice. *Immunology* **122**, 496–502 (2007). [doi:10.1111/j.1365-2567.2007.02676.x](https://doi.org/10.1111/j.1365-2567.2007.02676.x) [Medline](#)
- L. Kuo, P. S. Masters, Functional analysis of the murine coronavirus genomic RNA packaging signal. *J. Virol.* **87**, 5182–5192 (2013). [doi:10.1128/JVI.00100-13](https://doi.org/10.1128/JVI.00100-13) [Medline](#)
- K. Woo, M. Joo, K. Narayanan, K. H. Kim, S. Makino, Murine coronavirus packaging signal confers packaging to nonviral RNA. *J. Virol.* **71**, 824–827 (1997). [doi:10.1128/jvi.71.1.824-827.1997](https://doi.org/10.1128/jvi.71.1.824-827.1997) [Medline](#)
- J. A. Fosmire, K. Hwang, S. Makino, Identification and characterization of a coronavirus packaging signal. *J. Virol.* **66**, 3522–3530 (1992). [doi:10.1128/jvi.66.6.3522-3530.1992](https://doi.org/10.1128/jvi.66.6.3522-3530.1992) [Medline](#)
- A. Kanakan, N. Mishra, J. Srinivasa Vasudevan, S. Sahni, A. Khan, S. Sharma, R. Pandey, Threading the Pieces Together: Integrative Perspective on SARS-CoV-2. *Pathogens* **9**, 912 (2020). [doi:10.3390/pathogens9110912](https://doi.org/10.3390/pathogens9110912) [Medline](#)
- T. Giroglou, J. Cinatl Jr., H. Rabenau, C. Drosten, H. Schwalbe, H. W. Doerr, D. von Laer, Retroviral vectors pseudotyped with severe acute respiratory syndrome coronavirus S protein. *J. Virol.* **78**, 9007–9015 (2004). [doi:10.1128/JVI.78.17.9007-9015.2004](https://doi.org/10.1128/JVI.78.17.9007-9015.2004) [Medline](#)
- M. Ujike, C. Huang, K. Shirato, S. Makino, F. Taguchi, The contribution of the cytoplasmic retrieval signal of severe acute respiratory syndrome coronavirus to intracellular accumulation of S proteins and incorporation of S protein into virus-like particles. *J. Gen. Virol.* **97**, 1853–1864 (2016). [doi:10.1099/jgv.0.000494](https://doi.org/10.1099/jgv.0.000494) [Medline](#)
- X. Deng, M. A. Garcia-Knight, M. M. Khalid, V. Servellita, C. Wang, M. K. Morris, A. Sotomayor-González, D. R. Glasner, K. R. Reyes, A. S. Gliwa, N. P. Reddy, C. Sanchez San Martin, S. Federman, J. Cheng, J. Balcerak, J. Taylor, J. A. Streithorst, S. Miller, B. Sreeksumar, P.-Y. Chen, U. Schulze-Gahmen, T. Y. Taha, J. M. Hayashi, C. R. Simoneau, G. R. Kumar, S. McMahon, P. V. Lidsky, Y. Xiao, P. Hemarajata, N. M. Green, A. Espinosa, C. Kath, M. Haw, J. Bell, J. K. Hacker, C. Hanson, D. A. Wadford, C. Anaya, D. Ferguson, P. A. Frankino, H. Shivram, L. F. Lareau, S. K. Wyman, M. Ott, R. Andino, C. Y. Chiu, Transmission, infectivity, and neutralization of a spike L452R SARS-CoV-2 variant. *Cell* **184**, 3426–3437.e8 (2021). [doi:10.1016/j.cell.2021.04.025](https://doi.org/10.1016/j.cell.2021.04.025) [Medline](#)
- A. Kuzmina, Y. Khalaila, O. Voloshin, A. Keren-Naus, L. Boehm-Cohen, Y. Raviv, Y. Shemer-Avni, E. Rosenberg, R. Taube, SARS-CoV-2 spike variants exhibit differential infectivity and neutralization resistance to convalescent or post-

- vaccination sera. *Cell Host Microbe* **29**, 522–528.e2 (2021). [doi:10.1016/j.chom.2021.03.008](https://doi.org/10.1016/j.chom.2021.03.008) [Medline](#)
27. Y. Liu, J. Liu, K. S. Plante, J. A. Plante, X. Xie, X. Zhang, Z. Ku, Z. An, D. Scharlton, C. Schindewolf, V. D. Menachery, P.-Y. Shi, S. C. Weaver, The N501Y spike substitution enhances SARS-CoV-2 transmission. *bioRxiv* (2021). [doi:10.1101/2021.03.08.434499](https://doi.org/10.1101/2021.03.08.434499).
 28. C. Motozono, M. Toyoda, J. Zahradnik, A. Saito, H. Nasser, T. S. Tan, I. Ngare, I. Kimura, K. Uriu, Y. Kosugi, Y. Yue, R. Shimizu, J. Ito, S. Torii, A. Yonekawa, N. Shimono, Y. Nagasaki, R. Minami, T. Toya, N. Sekiya, T. Fukuhara, Y. Matsuura, G. Schreiber, T. Ikeda, S. Nakagawa, T. Ueno, K. Sato: Genotype to Phenotype Japan (G2P-Japan) Consortium, SARS-CoV-2 spike L452R variant evades cellular immunity and increases infectivity. *Cell Host Microbe* **29**, 1124–1136.e11 (2021). [doi:10.1016/j.chom.2021.06.006](https://doi.org/10.1016/j.chom.2021.06.006) [Medline](#)
 29. R. Kalker, Z. Cai, S. Lin, J. Farmer, Y. V. Kuzmichev, F. Koide, SARS-CoV-2 Spike Pseudoviruses: A Useful Tool to Study Virus Entry and Address Emerging Neutralization Escape Phenotypes. *Microorganisms* **9**, 1744 (2021). [doi:10.3390/microorganisms9081744](https://doi.org/10.3390/microorganisms9081744) [Medline](#)
 30. Y. Weisblum, F. Schmidt, F. Zhang, J. DaSilva, D. Poston, J. C. Lorenzi, F. Muecksch, M. Rutkowska, H.-H. Hoffmann, E. Michailidis, C. Gaebler, M. Agudelo, A. Cho, Z. Wang, A. Gazumyan, M. Cipolla, L. Luchsinger, C. D. Hillyer, M. Caskey, D. F. Robbiani, C. M. Rice, M. C. Nussenzweig, T. Hatziioannou, P. D. Bieniasz, Escape from neutralizing antibodies by SARS-CoV-2 spike protein variants. *eLife* **9**, e61312 (2020). [doi:10.7554/eLife.61312](https://doi.org/10.7554/eLife.61312) [Medline](#)
 31. W. T. Harvey, A. M. Carabelli, B. Jackson, R. K. Gupta, E. C. Thomson, E. M. Harrison, C. Ludden, R. Reeve, A. Rambaut, S. J. Peacock, D. L. Robertson; COVID-19 Genomics UK (COG-UK) Consortium, SARS-CoV-2 variants, spike mutations and immune escape. *Nat. Rev. Microbiol.* **19**, 409–424 (2021). [doi:10.1038/s41579-021-00573-0](https://doi.org/10.1038/s41579-021-00573-0) [Medline](#)
 32. X. Ju, Y. Zhu, Y. Wang, J. Li, J. Zhang, M. Gong, W. Ren, S. Li, J. Zhong, L. Zhang, Q. C. Zhang, R. Zhang, Q. Ding, A novel cell culture system modeling the SARS-CoV-2 life cycle. *PLOS Pathog.* **17**, e1009439 (2021). [doi:10.1371/journal.ppat.1009439](https://doi.org/10.1371/journal.ppat.1009439) [Medline](#)
 33. C. R. Carlson, J. B. Asfaha, C. M. Ghent, C. J. Howard, N. Hartoon, M. Safari, A. D. Frankel, D. O. Morgan, Phosphoregulation of Phase Separation by the SARS-CoV-2 N Protein Suggests a Biophysical Basis for its Dual Functions. *Mol. Cell* **80**, 1092–1103.e4 (2020). [doi:10.1016/j.molcel.2020.11.025](https://doi.org/10.1016/j.molcel.2020.11.025) [Medline](#)
 34. S. Lu, Q. Ye, D. Singh, Y. Cao, J. K. Diedrich, J. R. Yates 3rd, E. Villa, D. W. Cleveland, K. D. Corbett, The SARS-CoV-2 nucleocapsid phosphoprotein forms mutually exclusive condensates with RNA and the membrane-associated M protein. *Nat. Commun.* **12**, 502 (2021). [Medline](#)
 35. B. Li, A. Deng, K. Li, Y. Hu, Z. Li, Q. Xiong, Z. Liu, Q. Guo, L. Zou, H. Zhang, M. Zhang, F. Ouyang, J. Su, W. Su, J. Xu, H. Lin, J. Sun, J. Peng, H. Jiang, P. Zhou, T. Hu, M. Luo, Y. Zhang, H. Zheng, J. Xiao, T. Liu, R. Che, H. Zeng, Z. Zheng, Y. Huang, J. Yu, L. Yi, J. Wu, J. Chen, H. Zhong, X. Deng, M. Kang, O. G. Pybus, M. Hall, K. A. Lythgoe, Y. Li, J. Yuan, J. He, J. Lu, Viral infection and Transmission in a large well-traced outbreak caused by the Delta SARS-CoV-2 variant, *medRxiv* (2021); [doi:10.1101/2021.07.07.21260122](https://doi.org/10.1101/2021.07.07.21260122).

ACKNOWLEDGMENTS

We thank Dr. Pei-Yong Shi for providing the plasmids for SARS-CoV-2 reverse genetics. We would also like to acknowledge Dr. Jennifer Hamilton for advice and guidance and Dr. Stacia Wyman and Bryan Bach for sequencing of infectious clones. We thank Satish Pillai and Hannah S. Sperbert at Vitalant Research Institute (San Francisco, CA) for providing the 293T-ACE2-TMPRSS2 cells used for pseudovirus entry assays. We thank Sean P.J. Whelan lab for providing Vero cells overexpressing human TMPRSS2. We also thank Olivier Schwartz from Institut Pasteur for providing A549 cells stably expressing ACE2 (A549-ACE2). We thank Karl-Klaus Conzelmann for providing BSR-T7/5 cells. **Funding:** This project was funded by a grant from the National Institutes of Health (R21AI59666) and by support from the Howard Hughes Medical Institute and the Gladstone Institutes. AMS acknowledges the support of the Natural Sciences and Engineering Research Council of Canada (NSERC PDF-533021-2019) and IPC support from the NIH (F31 AI164671-01). **Author contributions:** Conceptualization: AMS, JAD. Investigation: AMS, TYT, TT, IPC, AC, MMK, BS, P-YC, JMH, KMS. Methodology: AMS, TYT, TT, JAD, MO. Supervision: JAD, MO.

Writing: AMS, TYT, TT, JAD. **Competing interests:** AMS and JAD are inventors on a patent application filed by the Gladstone Institutes and the University of California that covers the method and composition of SARS-CoV-2 VLP preparations for RNA transduction and expression in cells. **Data and materials availability:** All data are available in the main paper or supplementary material. Plasmids are available from Addgene (addgene.org) or by request. This work is licensed under a Creative Commons Attribution 4.0 International (CC BY 4.0) license, which permits unrestricted use, distribution, and reproduction in any medium, provided the original work is properly cited. To view a copy of this license, visit <https://creativecommons.org/licenses/by/4.0/>. This license does not apply to figures/photos/artwork or other content included in the article that is credited to a third party; obtain authorization from the rights holder before using such material.

SUPPLEMENTARY MATERIALS

science.org/doi/10.1126/science.abl6184

Materials and Methods

Figs. S1 to S6

Tables S1 to S3

References

MDAR Reproducibility Checklist

26 July 2021; accepted 29 October 2021

Published online 4 November 2021

10.1126/science.abl6184

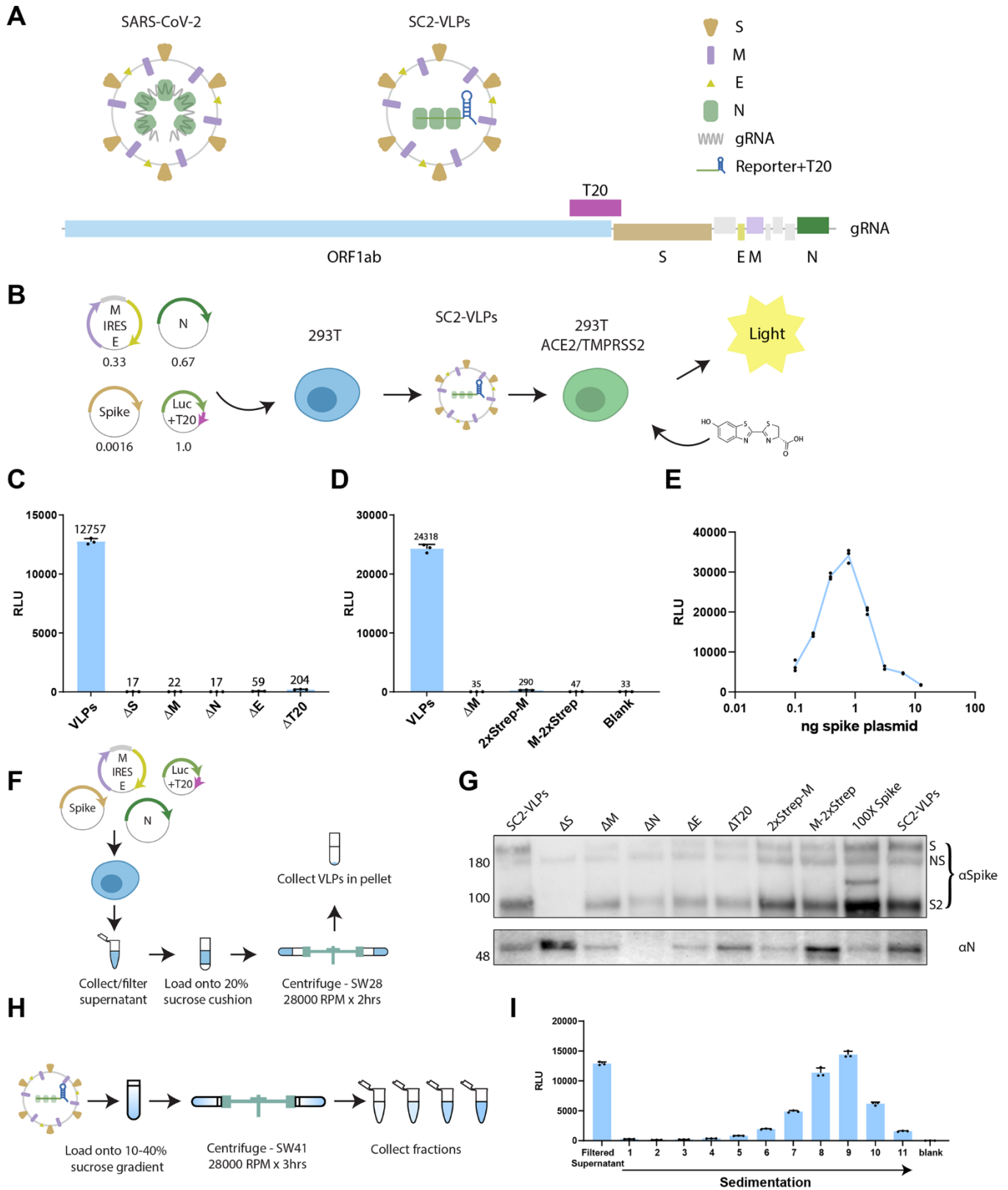
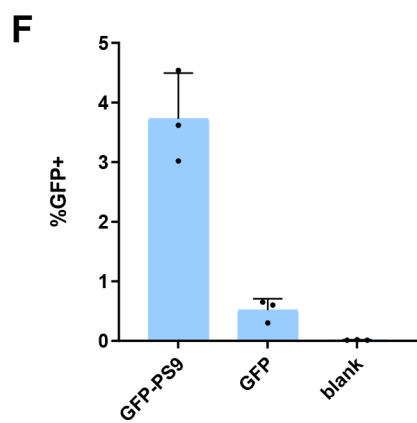
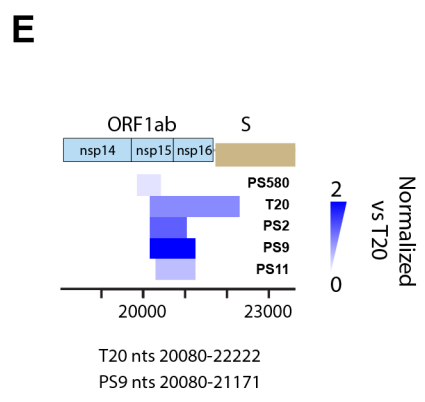
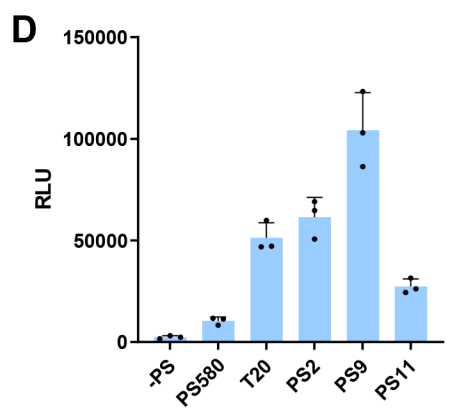
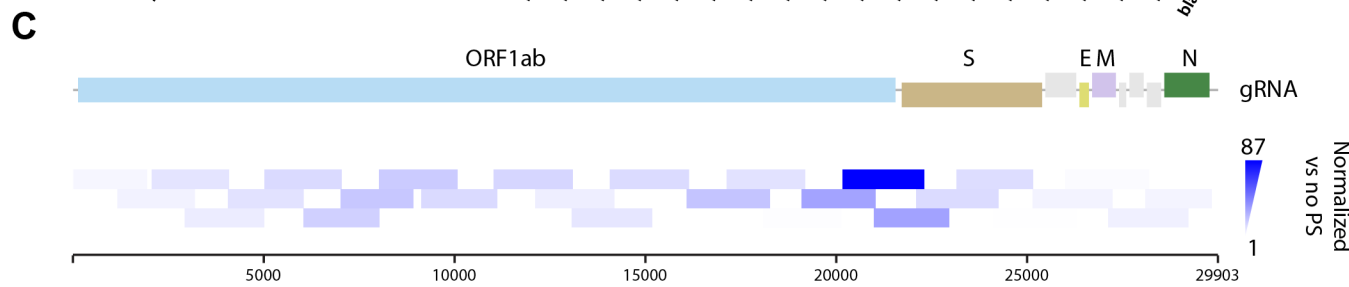
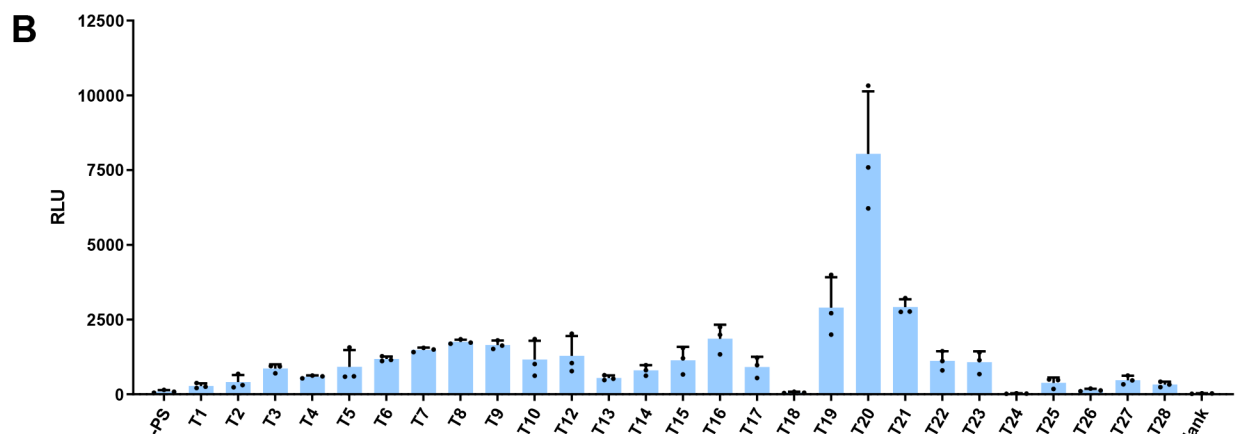
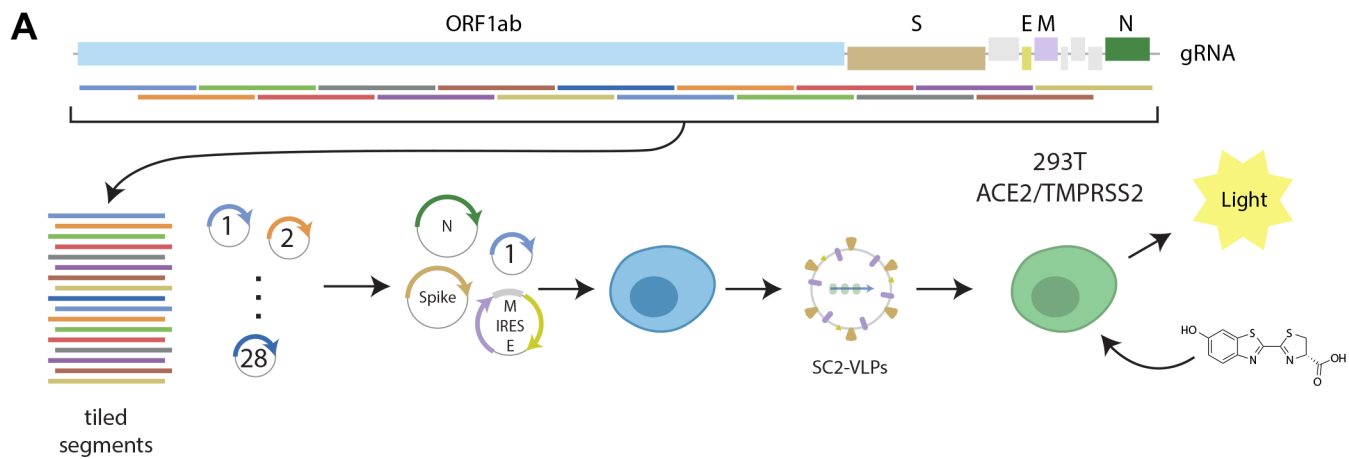


Fig. 1 (previous page). Design and characterization of SC2-VLPs. (A) Schematic of SARS-CoV-2 and SC2-VLP design and location of RNA packaging sequence T20. (B) Process for generating and detecting luciferase encoding SC2-VLPs. Numbers below plasmid maps indicate ratios used for transfection. (C) Induced luciferase expression measured in receiver cells (293T-ACE2/TMPRSS2) from “Standard” SC2-VLPs containing S, M, N, E and luciferase-T20 transcript as well as VLPs lacking each one of the components. (D) N- or C-terminal 2x strep-tag on M abrogates vector induced luciferase expression. (E) Optimal luciferase expression requires a narrow range of spike plasmid concentrations corresponding to 1/500th of the total plasmid mass used for transfection. (F) Schematic for purification of SC2-VLPs. (G) Western blot showing S and N in pellets purified from standard SC2-VLPs and conditions that did not induce luciferase expression in receiver cells. (H) Schematic for sucrose gradient for separating SC2-VLPs. (I) Induced luciferase expression from sucrose gradient fractions of SC2-VLPs. S2: Cleavage product of S. NS: Non-specific band. Error bars indicate standard deviation with N = 3 independent transfections in each case.

Fig. 2 (next page). RNA packaging into SC2-VLPs by SARS-CoV-2 sequences. (A) Arrayed screen for determining the location of the optimal sequence for RNA packaging in SC2-VLPs. 2-kb tiled segments of the genome were cloned into the 3' UTR of the luciferase plasmid. (B) Induced luciferase expression in receiver cells by SC2-VLPs containing different tiled segments from the SARS-CoV-2 genome. (C) Heatmap visualization of the data from (B) showing the locations of tiled segments relative to the SARS-CoV-2 genome. Color intensity indicates luminescence of receiver cells for each tile normalized to expression for luciferase plasmid containing no insert. (D) Smaller segments of the genome were used to locate the optimal RNA packaging sequence. (E) Heatmap visualization of the data from (D). (F) Flow cytometry analysis of GFP expression in 293T ACE2/TMPRSS2 cells incubated with SC2-VLPs encoding GFP-PS9, GFP (no packaging sequence) or no VLPs. Error bars indicate standard deviation with N = 3 independent transfections in each case.



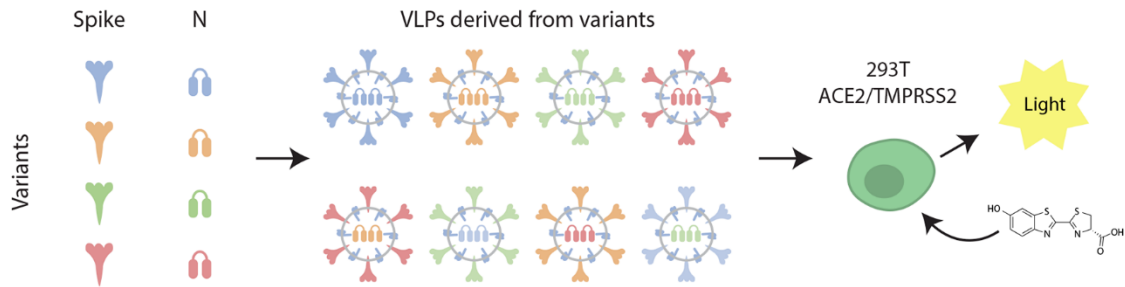
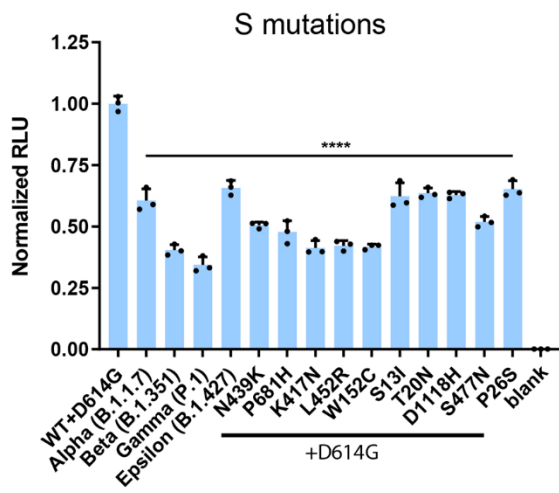
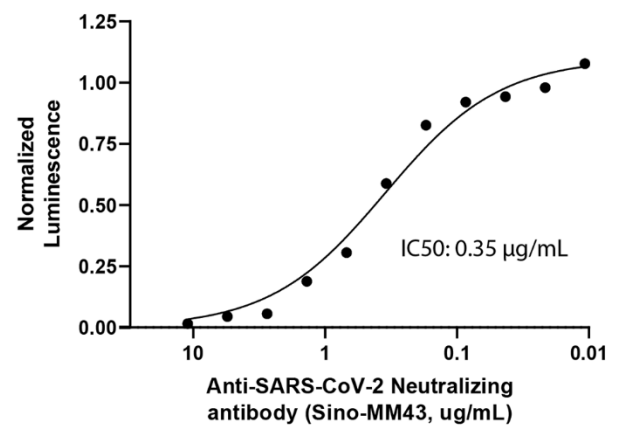
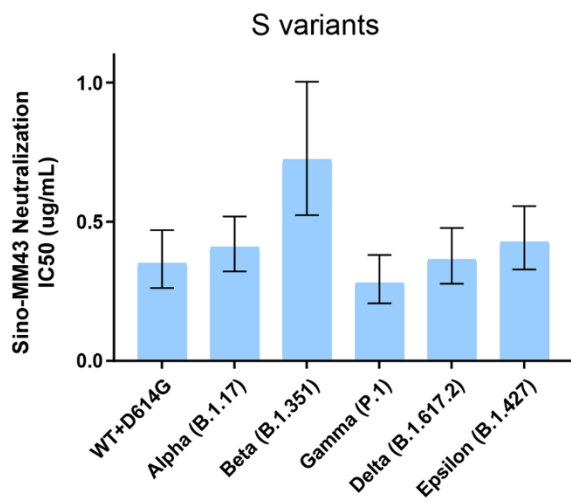
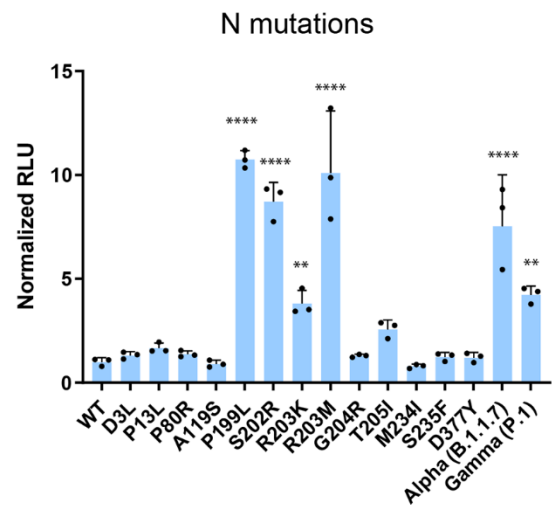
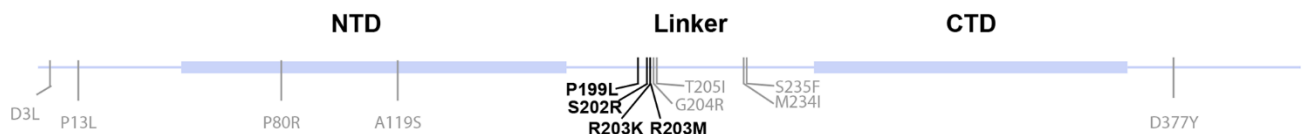
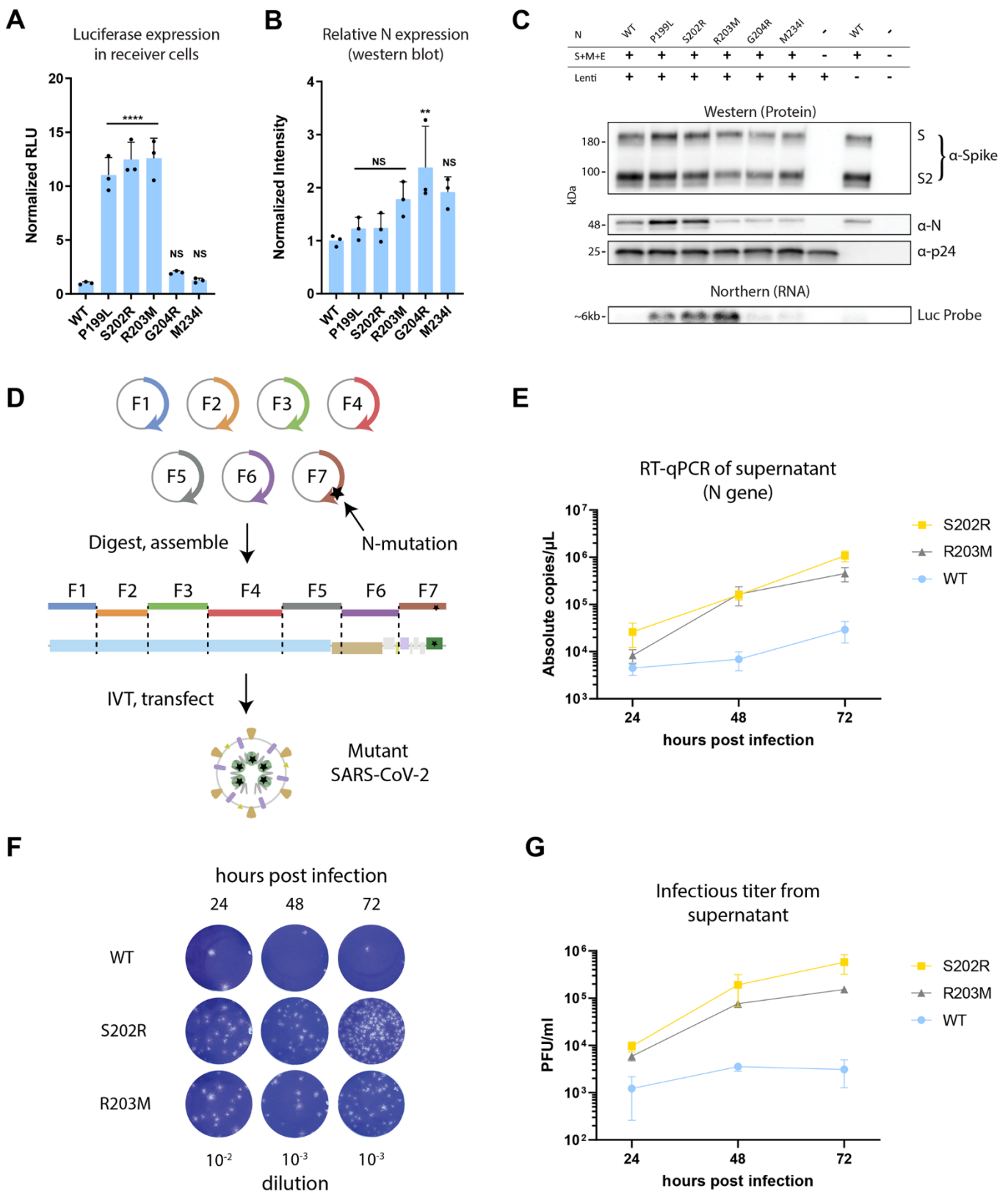
A**B****C****D****E****F**

Fig. 3 (previous page). Effect of mutations in the S and N proteins on SC2-VLP induced luminescence. (A) Schematic for cloning and testing mutations observed in SARS-CoV-2 variants using SC2-VLPs. (B) Initial screen of 15 S mutants compared to a reference ancestral S containing the D614G mutation (termed WT). Details of mutations listed in table S2. (C) Neutralization curve for SC2-VLPs generated using ancestral S and neutralized with anti-S antibody MM43 (SinoBiological, cat# 40591). (D) Neutralization IC50 of S variants using SC2-VLPs and MM43. (E) Initial screen of 15 N mutants compared to the reference Wuhan Hu-1 N sequence (WT). Details of mutations listed in table S3. (F) Map of SARS-CoV-2 N domains showing the locations of observed mutations. Mutations observed to enhance signal are bolded. (B and E) Error bars indicate standard deviation with N = 3 independent transfections in each case. Significance was determined by one-way analysis of variance and multiple comparisons using Holm-Šídák test. **p < 0.01, ****p < 0.0001. (E) Error bars indicate 95% confidence intervals derived from curve fitting in Graphpad Prism.

Fig. 4 (next page). Impact of mutations in SARS-CoV-2 N on RNA packaging and viral titer. (A) Luciferase expression in receiver cells from six N mutants re-tested after preparation in a larger batch. (B) Relative N-expression of selected mutants in packaging cells normalized to WT using GAPDH as a loading control. (C) Western blot (protein) and Northern blot (RNA) of VLPs generated using N-mutants purified by ultracentrifugation. Lentivirus was added before ultracentrifugation to allow utilization of p24 as an internal control. (D) Schematic for reverse genetics system used to generate mutant SARS-CoV-2. (E) RT-qPCR of supernatant collected from A549-ACE2 cells infected with WT and mutant SARS-CoV-2 at MOI of 0.1 at 24, 48, and 72 hours post infection. (F) Representative plaques and (G) quantification of infectious viral titers from the same experiment. MOI: Multiplicity of infection; CTD: C-terminal domain. Error bars indicate standard deviation with N = 3 independent transfections/infections in each case. Significance was determined by one-way analysis of variance and multiple comparisons using Holm-Šídák test. **p < 0.01, ****p < 0.0001.



Rapid assessment of SARS-CoV-2 evolved variants using virus-like particles

Abdullah M. SyedTaha Y. TahaTakako Tabatalrene P. ChenAlison CilingMir M. KhalidBharath SreekumarPei-Yi ChenJennifer M. HayashiKatarzyna M. SoczekMelanie OttJennifer A. Doudna

Science, Ahead of Print

View the article online

<https://www.science.org/doi/10.1126/science.abl6184>

Permissions

<https://www.science.org/help/reprints-and-permissions>

Use of think article is subject to the [Terms of service](#)



Supplementary Materials for

Rapid assessment of SARS-CoV-2 evolved variants using virus-like particles

Abdullah M. Syed *et al.*

Corresponding authors: Email: Jennifer A. Doudna, doudna@berkeley.edu;
Melanie Ott, melanie.ott@gladstone.ucsf.edu

DOI: [10.1126/science.abl6184](https://doi.org/10.1126/science.abl6184)

The PDF file includes:

Materials and Methods
Figs. S1 to S6
Tables S1 to S3
References

Other Supplementary Material for this manuscript includes the following:

MDAR Reproducibility Checklist

Materials and methods

Cloning for plasmids encoding structural proteins: pcDNA3.1 backbone plasmids were generated encoding N, and M-IRES-E. Sequences for E, M and N were PCR amplified from codon optimized plasmids were gifts from Nevan Krogan (Addgene plasmid # 141385, 141386, 141391,). pcDNA3.1-SARS2-Spike was a gift from Fang Li (Addgene plasmid # 145032). Site directed mutagenesis (NEB) was used to remove the C9-tag and introduce the D614G mutation.

Cloning of SARS-CoV-2 genome tiled segments: RNA was extracted from SARS-CoV-2 (Washington isolate) viral supernatant inactivated in Trizol by phase separation. RNA was reverse transcribed using protoscript II (NEB) and tiled segments (T1-T28) were PCR amplified from cDNA using primers compatible with ligation independent cloning (LIC). Tiles were cloned into a plasmid containing luciferase with a LIC destination site in the 3'UTR.

SC2-VLP production: For a 6-well, plasmids Cov2-N (0.67), CoV2-M-IRES-E (0.33), CoV2-Spike (0.0016) and Luc-T20 (1.0) at indicated mass ratios for a total of 4 µg of DNA were diluted in 200 µL optimem. 12 µg PEI was diluted in 200 µL Opti-MEM and added to plasmid dilution quickly to complex the DNA. Transfection mixture was incubated for 20 minutes at room temperature and then added dropwise to 293T cells in 2 mL of DMEM containing fetal bovine serum and penicillin/streptomycin. Media was changed after 24 hours of transfection and At 48 hours post-transfection, VLP containing supernatant was collected and filtered using a 0.45 µm syringe filter. For other culture sizes, the mass of DNA used was 1 µg for 24-well, 4 µg for 6-well, 20 µg for 10-cm plate and 60 µg for 15-cm plate. Optimem volumes were 100 µL, 400 µL, 1 mL and 3 mL respectively and PEI was always used at 3:1 mass ratio.

Luciferase readout: In each well of a clear 96-well plate 50 µL of SC2-VLP containing supernatant was added to 50 µL of cell suspension containing 30 000 receiver cells (293T

ACE2/TMPRSS2). Cells were allowed to attach and take up VLPs overnight. Next day, supernatant was removed and cells were rinsed with 1X PBS and lysed in 20 μ L passive lysis buffer (Promega) for 15 minutes at room temperature with gentle rocking. Lysates were transferred to an opaque white 96-well plate and 50 μ L of reconstituted luciferase assay buffer was added and mixed with each lysate. Luminescence was measured immediately after mixing using a TECAN plate reader.

SC2-VLP purification using sucrose cushion: SC2-VLP produced in 10-cm plates (10 mL of culture) were added to 13.2 mL ultracentrifuge tubes. 1 mL of 20% sucrose was underlaid using a 4" blunt needle. VLPs were centrifuged for 2 hours at 28 000 RPM using a SW41 Ti swinging bucket rotor. Supernatant was removed and ultracentrifuge tubes were inverted for 5 minutes on a paper towel with gentle tapping to remove remaining supernatant. VLPs were resuspended in 50 μ L phosphate buffered saline for further experiments.

SC2-VLP PEG precipitation: 0.136 volumes of polyethylene glycol stock (50% PEG, 2.2% NaCl) was added to filtered supernatants containing SC2-VLPs to achieve a final concentration of 6% PEG. Solution was mixed thoroughly and precipitation was allowed to proceed for 2hrs at 4°C and then centrifuged at 2 000g for 20 minutes. Supernatant was discarded and VLPs were resuspended in PBS.

SC2-VLP concentration using Amicon filters: 0.5 mL filtered supernatant was added to 0.5 mL 100 kDa molecular weight cutoff amicon filters and centrifuged for 30 minutes at 2 000g.

Concentrate was diluted in 1X PBS containing 0.02% Tween 20 for all wash steps.

Western blot: For western blots of lysates, media was removed and cells were rinsed with PBS. Cells were then lysed for 20 minutes in RIPA lysis buffer containing Halt protease and phosphatase inhibitor cocktail. For western blots of ultracentrifuge concentrated VLPs, 10 mL of

VLP supernatant from a 10-cm plate was pelleted (28 000 RPM, 2hrs, SW41 Ti, 1mL 20% sucrose cushion), the supernatant was discarded and VLPs were resuspended in 50 μ L of PBS. 15 μ L of concentrated VLPs were used to western blot. Laemmli loading buffer (1x final) and dithiothreitol (DTT, 40 mM final) was added to lysates or VLP solution and heated for 95°C for 5 minutes to lyse VLPs and denature proteins. Samples were loaded on to 12-40% gradient gels (Biorad) and transferred to a PVDF membrane (Biorad). Membrane was blocked in 10% NFDM and stained with primary antibody: anti-N (abcam ab273434, 1:500 dilution), anti-S (abcam ab272504, 1:1000), anti-GAPDH (Santa Cruz sc-365062, 1:1000), anti-p24 (Sigma, 1:2000) for 2 hours at room temperature. Blots were rinsed with TBS-T three times for 10 minutes each and stained with secondary (abcam ab205719 (mouse), 1:5000). Imaged using pierce chemiluminescence kit.

Sucrose gradient fractionation: 10% to 40% sucrose gradient was prepared using a gradient mixer in 13.2 mL ultracentrifuge tubes. Concentrated and resuspended SC2-VLPs were overlaid on top of the gradient and centrifuged in a SW41 Ti rotor for 3 hours at 28 000 RPM. Gradient was fractionated from the bottom using a 4" blunt needle and a peristaltic pump. For cell infection, each fraction was diluted 20X and added to 293T cells expressing ACE2/TMPRSS2. Luciferase signal was measured the next day.

GFP-VLPs and flow cytometry. GFP was cloned into the luciferase destination vector (Luc-no PS) and Luc-PS9 to generate GFP-LIC and GFP-PS9. VLPs were generated in 10-cm plates and concentrated through a 20% sucrose cushion. 50 μ L of concentrated VLPs were added to each well of a 24-well plate along with 120 000 receiver cells (293T ACE2/TMPRSS2). Cells were incubated with VLPs overnight and GFP expression was measured the next day using flow cytometry.

Northern Blot: VLPs collected from a 10-cm plate were concentrated by ultracentrifugation through a 20% sucrose cushion (28 000 RPM, 2hrs, SW41 Ti). The supernatant was discarded and VLPs were resuspended in 50 μ L of PBS. 20 μ L of concentrated VLPs were used for Northern blotting. VLPs were lysed by adding 500 μ L of Trizol (Sigma) and RNA was extracted by phase separation, precipitated with isopropanol with GlycoBlue and washed with 75% ethanol. RNA was resuspended in 30 μ L of water, added to 30 μ L 2x RNA Loading Dye (NEB) and denatured at 65°C for 15 minutes then loaded onto a 1% agarose gel containing 1X MOPS and 4% formaldehyde. Samples were run at room temperature for 12hrs at 20V and transferred by capillary action to Nylon membrane. The membrane was hybridized with a ³²P-labeled luciferase DNA probe (Promega) and visualized using a phosphoscreen on a Typhoon imager (GE).

Construction of SARS-CoV2 mutant viruses: Seven cDNA fragments spanning the USA/WA1-2020 SARS-CoV-2 genome were a kind gift from Dr. Pei-Yong Shi. SARS-CoV2 nucleocapsid S202R and R203M mutant viruses were constructed by mutagenesis of a previously described seven-fragment cDNA clone USA/WA1-2020 SARS-CoV-2 (4). Briefly, N:S202R and N:R203M mutations were introduced into fragment 7 (F7) (pCC1-CoV2-F7) using site-directed mutagenesis. To assemble the full length SARS-CoV2 cDNA, cDNA fragments were obtained by restriction enzyme digestion (BsaI for F1-4 and Esp3I/PvuI for F5-6 and Esp3I/SnaBI for F7), and purification by gel extraction (Qiagen gel extraction kit). In vitro ligation of the fragments was done in three steps: 1) ligation of F1-3, F4-5, and F6-7 separately; 2) ligation of F1-3 and F4-5 to obtain F1-5; 3) ligation of F1-5 to F6-7 to obtain F1-7. All ligations were performed with T4 DNA ligase overnight at 4°C. The full length F1-7 cDNA was phenol/chloroform extracted, isopropanol precipitated, and resuspended in nuclease-free water. SARS-CoV2 full length gRNA

was produced by using mMACHINE T7 Transcription Kit (ThermoFisher Scientific). The purified SARS-CoV2 full length wild type and mutant gRNAs were electroporated into BSR-T7/T5 cells, which are baby hamster kidney-21 (BHK-21) cells constitutively expressing T7 RNA polymerase and co-cultured with Vero-TMPRSS2 cells along with WT N RNA. After 3-4 days or until CPE is observed, mutant viruses (P0) were collected and used to infect Vero-TMPRSS2 cells to produce P1 viral stocks that were utilized for subsequent infection experiments. All viral sequences were verified by NGS (fig. S6). Viral titers were determined by plaque assays on Vero-TMPRSS2 cells. Virus preparation and experiments were performed in the BSL3 facility.

Cell lines: Cells were maintained in a humidified incubator at 37°C in 5% CO₂ in the indicated media and passaged every 3-4 days. 293T cells were obtained from ATCC and maintained in DMEM with 10% FBS and 1% penicillin/streptomycin. 293T-ACE2/TMPRSS2 were a gift from Satish Pillai lab and cultured in DMEM with 10% FBS, 1% P/S, 2 µg/ml puromycin and 10 µg/ml blasticidin. Vero E6 was cultured in DMEM supplemented with 10% FBS and 2mM glutamine. Vero cells overexpressing human TMPRSS2, a kind gift from the Whelan lab (Case et al., 2020), were grown in DMEM with 10% FBS and 1x glutamine. A549 cells stably expressing ACE2 (A549-ACE2) were a gift from O. Schwartz. A549-ACE2 cells were cultured in DMEM supplemented with 10% FBS, 2mM glutamine and blasticidin (20 µg/ml) (Sigma). Short Terminal Repeat (STR) analysis by the Berkeley Cell Culture Facility on 17 July 2020 authenticates these as A549 cells with 100% probability.

Infection and titration of infectious clones: A549-ACE2 were inoculated with WT, S202R, or R203M mutant viruses at multiplicity of infection (MOI) 0.1 in triplicate for 1 hr. After the infection, the cells were washed with PBS to remove the unattached virus and then cultured for

72 hours. Medium was changed and cell culture supernatants were collected daily and stored -80°C for virus titration by plaque assay. Cells and cell culture supernatants were also collected for RNA analysis.

Plaque assays: Vero-TMPRSS2 were plated 2.5×10^5 cells per well in 12-well plates overnight. Cell culture supernatants were serially diluted in DMEM with 10% FBS and 300 μ l of diluted inoculum were added to Vero-TMPRSS2 monolayers at 37C, 5% CO₂ for 1 hr, followed by an Avicel (IMCD) overlay. After 3 days, plaques were fixed with 10% formalin and visualized by staining with crystal violet.

Supplementary Figure 1

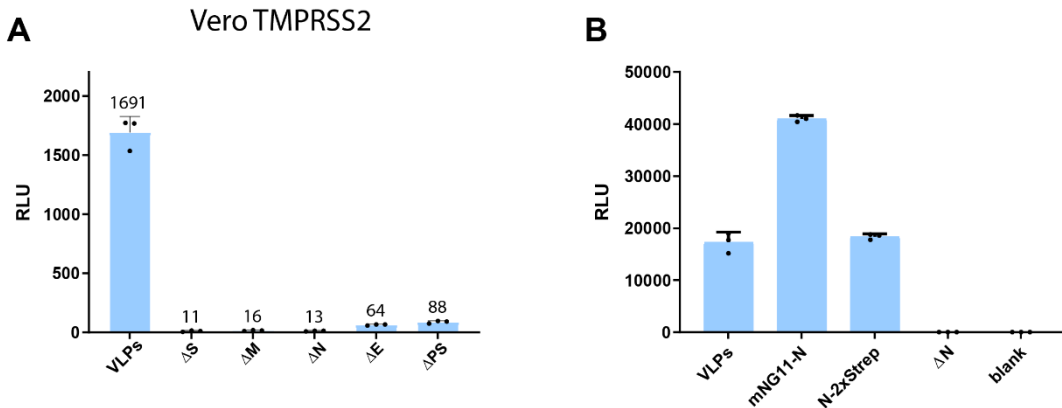


Fig. S1. Requirements for induced expression by SC2-VLPs. A) Luminescence measured from Vero E6 cells incubated with standard SC2-VLPs as well as missing either S, M, N, E or the packaging signal (PS). B) Luminescence from receiver cells after incubation with standard SC2-VLPs as well as tagged N (mNG11-N: N with amino-terminal mNG11 tag and N-2xStrep: N with carboxy-terminal 2xStrep tag). Error bars indicate standard deviation with N=3 independent transfections in each case.

Supplementary Figure 2

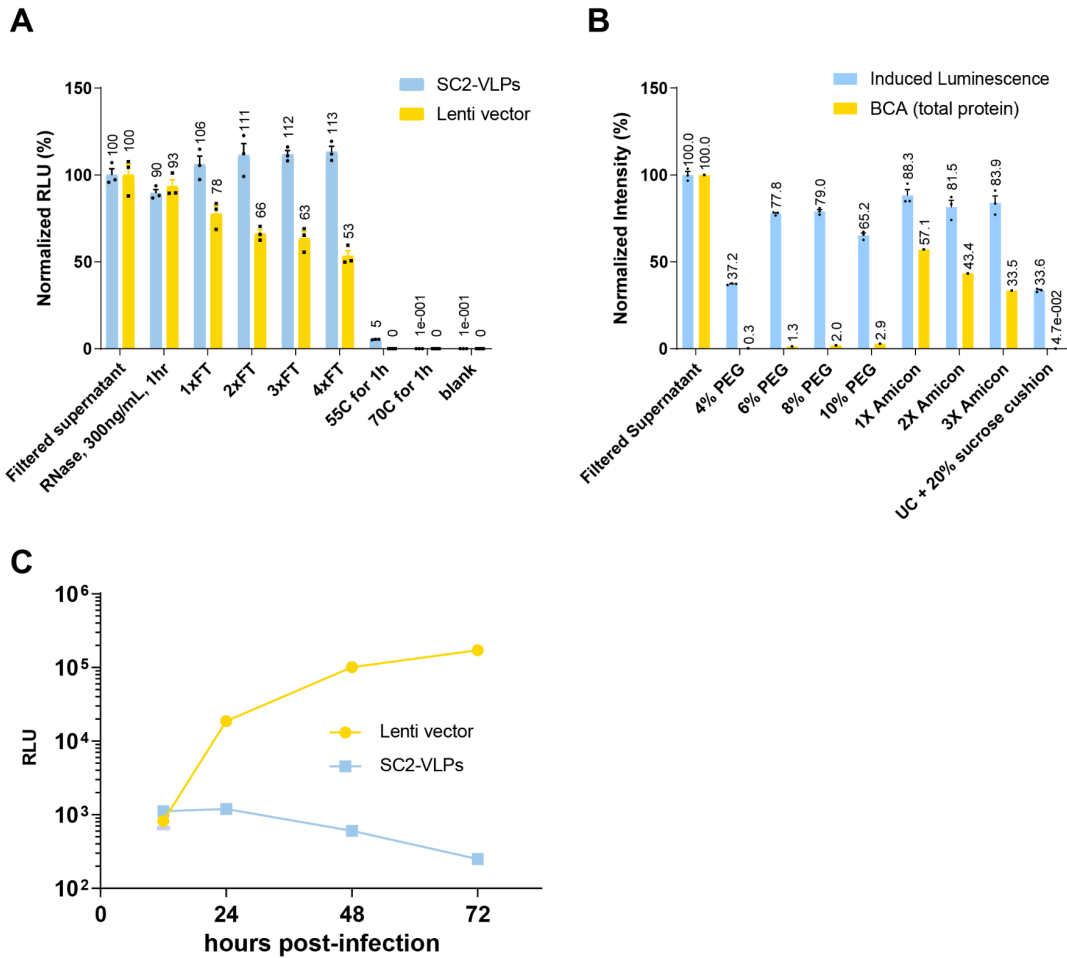


Fig. S2. Characterization of SC2-VLPs stability and purification. A) Luminescence induced in receiver cells from SC2-VLPs after treatment with ribonuclease A or 1-4 freeze-thaw cycles or incubation at 55°C and 70°C, respectively. All values were normalized to the original supernatant. Lentiviral particles encoding luciferase are shown as comparison. B) Induced luminescence from SC2-VLPs purified/concentrated using different methods compared to total protein measurement from the same samples using bicinchoninic acid (BCA) assay. C) Luminescence measured from 293T-AC2/TMPRSS2 receiver cells at 12, 24, 48, and 72 hours after incubation with either S-pseudotyped lentivirus or SC2-VLPs encoding luciferase. Error bars indicate standard deviation with N=3 independent transfections in each case.

Supplementary Figure 3

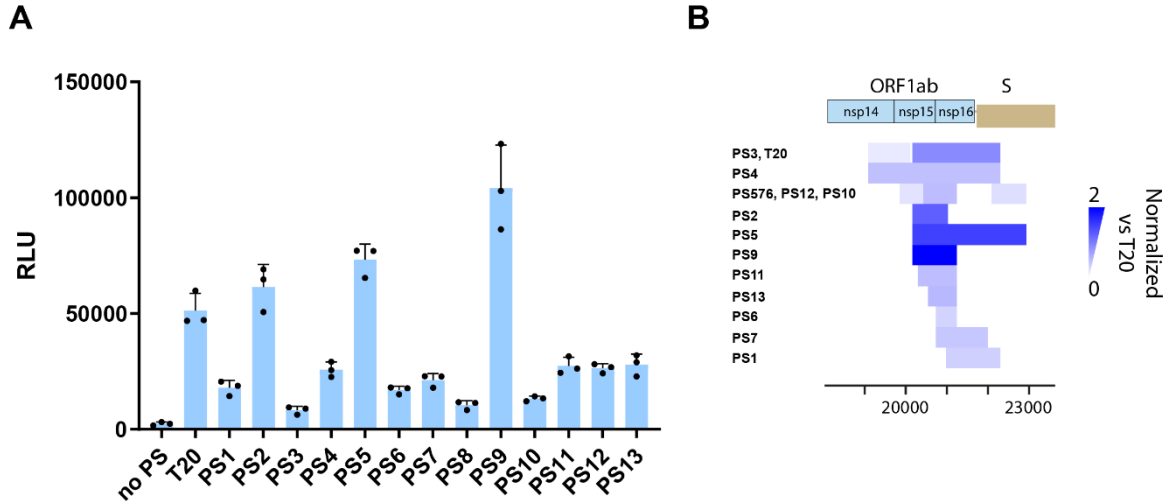


Fig. S3. Minimal sequence required for specific packaging into SC2-VLPs. A) Induced luminescence in receiver cells after incubation with SC2-VLPs containing a transcript expressing luciferase. The luciferase transcript contains varying segments from SARS-CoV-2 genome shown graphically in (B). “no PS” indicates luciferase only transcript. Color in (B) indicates the observed luminescence normalized to the T20 transcript. Error bars indicate standard deviation with N=3 independent transfections/infections in each case.

Supplementary Figure 4

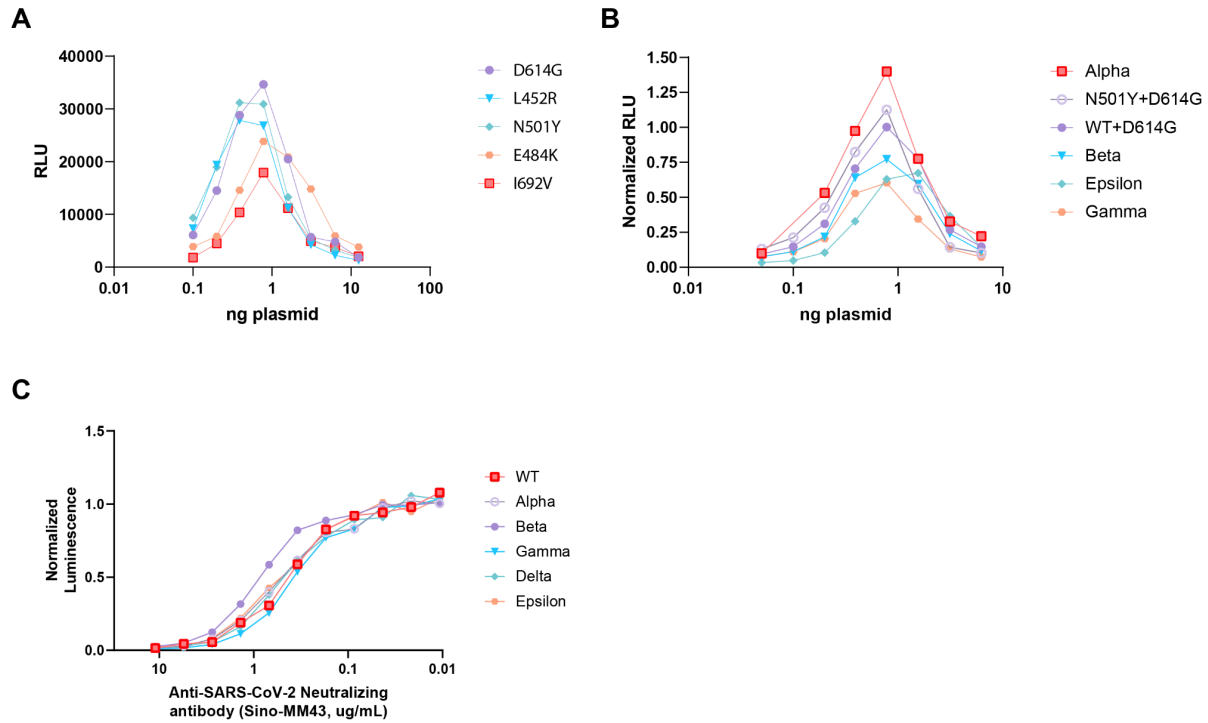


Fig. S4. Effect of spike mutations on SC2-VLPs and neutralization. A, B) Induced luminescence from receiver cells incubated with SC2-VLPs containing varying concentrations of and mutations within the S plasmid. S plasmid ranging from 0.1 ng to 12.5 ng was added to each well of a 24-well plate. Total DNA used for transfection (N, M-IRES-E, T20) was 1 μ g for each well. C) Neutralization curves of S variants against antibody MM43 (SinoBiological). IC₅₀ from each shown in Fig. 3D.

Supplementary Figure 5

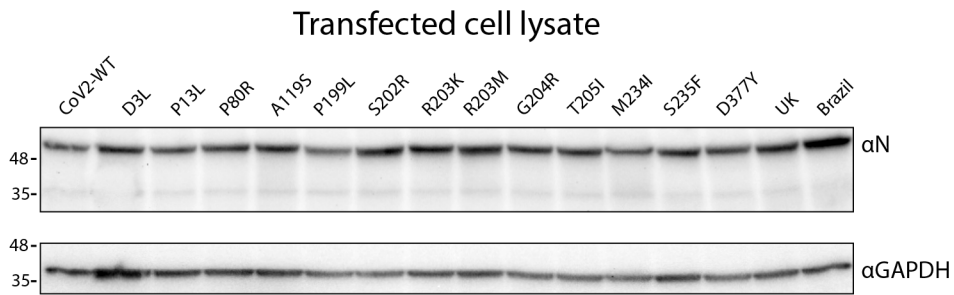


Fig. S5. Expression levels of N mutants. Western blot of lysates from packaging cells transfected with N mutations stained using anti-N antibody (top) and anti-GAPDH antibody (bottom). Expression levels are similar between mutants and do not correlate with induced luminescence from SC2-VLPs made from these mutants.

Supplementary Figure 6

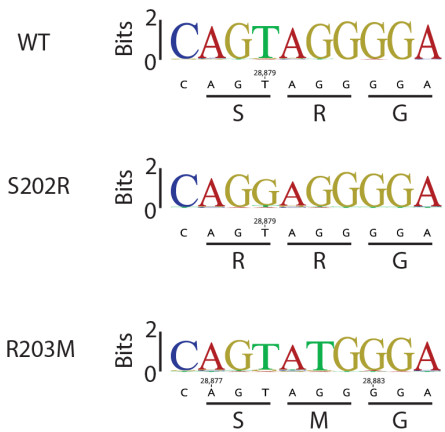


Fig. S6. Sequence logo visualization of sequencing data from infectious clones generated by reverse genetics. Arrows indicate sites that were modified.

Table S1. Nucleotide start and end positions of sequences T1-T28 and PS1-PS9 relative to the Wuhan Hu-1 reference genome.

Sequence name	Start position	End position
T1	18	1932
T2	1172	3179
T3	2070	4075
T4	2936	5010
T5	4054	6038
T6	5004	7020
T7	6018	8009
T8	6996	8898
T9	8006	10043
T10	9101	11072
T11	10013	12088
T12	11001	13055
T13	12074	14137
T14	13028	15133
T15	14010	16085
T16	16011	18186
T17	17068	19115
T18	18020	20047
T19	19018	20955
T20	20080	22222
T21	20912	22873
T22	22016	24166
T23	23050	25077
T24	24038	26169
T25	25056	27130
T26	25906	28096
T27	27029	29125
T28	27987	29727

PS1	20912	22221
PS2	20080	20954
PS3	19018	20046
PS4	19018	22221
PS5	20080	22872
PS6	20654	21171
PS7	20654	21920
PS8	19785	20348
PS9	20080	21171
PS10	22016	22872
PS11	20231	21171
PS12	20352	21171
PS13	20468	21171

Table S2. CoV-2 S mutations and variants screened relative to Wuhan Hu-1 reference genome.

Label	Mutations
WT+D614G	D614G
Alpha (B.1.1.7)	del69,70, del144, D614G, N501Y, A570D, P681H, T716I, S982A, D1118H
Beta (B.1.351)	K417N, E484K, N501Y, D614G
Gamma (P.1)	L13F, T20N, P26S, D138Y, R190S, K417T, E484K, N501Y, D614G, H655Y, T1027I, V1176F
Epsilon (B.1.427)	S13I, W152C, L452R, D614G
N439K	N439K, D614G
P681H	D614G, P681H
K417N	K417N, D614G
L452R	L452R, D614G
W152C	W152C, D614G
S13I	S13I, D614G
T20N	T20N, D614G
D1118H	D614G, D1118H

S477N	S477N, D614G
P26S	P26S, D614G

Table S3. CoV-2 N mutations and variants screened relative to Wuhan Hu-1 reference genome.

Label	Mutations
WT	
D3L	D3L
P13L	P13L
P80R	P80R
A119S	A119S
P199L	P199L
S202R	S202R
R203K	R203K
R203M	R203M
G204R	G204R
T205I	T205I
M234I	M234I
S235F	S235F
D377Y	D377Y
Alpha	D3L, R203K, G204R, S235F
Gamma (P.1)	P80R, R203K, G204R

References and Notes

1. X. Xie, A. Muruato, K. G. Lokugamage, K. Narayanan, X. Zhang, J. Zou, J. Liu, C. Schindewolf, N. E. Bopp, P. V. Aguilar, K. S. Plante, S. C. Weaver, S. Makino, J. W. LeDuc, V. D. Menachery, P.-Y. Shi, An Infectious cDNA Clone of SARS-CoV-2. *Cell Host Microbe* **27**, 841–848.e3 (2020). [doi:10.1016/j.chom.2020.04.004](https://doi.org/10.1016/j.chom.2020.04.004) [Medline](#)
2. S. Torii, C. Ono, R. Suzuki, Y. Morioka, I. Anzai, Y. Fauzyah, Y. Maeda, W. Kamitani, T. Fukuhara, Y. Matsuura, Establishment of a reverse genetics system for SARS-CoV-2 using circular polymerase extension reaction. *Cell Rep.* **35**, 109014 (2021). [doi:10.1016/j.celrep.2021.109014](https://doi.org/10.1016/j.celrep.2021.109014) [Medline](#)
3. C. Ye, K. Chiem, J.-G. Park, F. Oladunni, R. N. Platt 2nd, T. Anderson, F. Almazan, J. C. de la Torre, L. Martinez-Sobrido, Rescue of SARS-CoV-2 from a Single Bacterial Artificial Chromosome. *mBio* **11**, e02168-20 (2020). [doi:10.1128/mBio.02168-20](https://doi.org/10.1128/mBio.02168-20) [Medline](#)
4. X. Xie, K. G. Lokugamage, X. Zhang, M. N. Vu, A. E. Muruato, V. D. Menachery, P.-Y. Shi, Engineering SARS-CoV-2 using a reverse genetic system. *Nat. Protoc.* **16**, 1761–1784 (2021). [doi:10.1038/s41596-021-00491-8](https://doi.org/10.1038/s41596-021-00491-8) [Medline](#)
5. S. J. Rihn, A. Merits, S. Bakshi, M. L. Turnbull, A. Wickenhagen, A. J. T. Alexander, C. Baillie, B. Brennan, F. Brown, K. Brunner, S. R. Bryden, K. A. Burness, S. Carmichael, S. J. Cole, V. M. Cowton, P. Davies, C. Davis, G. De Lorenzo, C. L. Donald, M. Dorward, J. I. Dunlop, M. Elliott, M. Fares, A. da Silva Filipe, J. R. Freitas, W. Furnon, R. J. Gestuevo, A. Geyer, D. Giesel, D. M. Goldfarb, N. Goodman, R. Gunson, C. J. Hastie, V. Herder, J. Hughes, C. Johnson, N. Johnson, A. Kohl, K. Kerr, H. Leech, L. S. Lello, K. Li, G. Lieber, X. Liu, R. Lingala, C. Loney, D. Mair, M. J. McElwee, S. McFarlane, J. Nichols, K. Nomikou, A. Orr, R. J. Orton, M. Palmarini, Y. A. Parr, R. M. Pinto, S. Raggett, E. Reid, D. L. Robertson, J. Royle, N. Cameron-Ruiz, J. G. Shepherd, K. Smollett, D. G. Stewart, M. Stewart, E. Sugrue, A. M. Szemiel, A. Taggart, E. C. Thomson, L. Tong, L. S. Torrie, R. Toth, M. Varjak, S. Wang, S. G. Wilkinson, P. G. Wyatt, E. Zusinaite, D. R. Alessi, A. H. Patel, A. Zaid, S. J. Wilson, S. Mahalingam, A plasmid DNA-launched SARS-CoV-2 reverse genetics system and coronavirus toolkit for COVID-19 research. *PLOS Biol.* **19**, e3001091 (2021). [doi:10.1371/journal.pbio.3001091](https://doi.org/10.1371/journal.pbio.3001091) [Medline](#)
6. J. A. Plante, Y. Liu, J. Liu, H. Xia, B. A. Johnson, K. G. Lokugamage, X. Zhang, A. E. Muruato, J. Zou, C. R. Fontes-Garfias, D. Mirchandani, D. Scharton, J. P. Bilello, Z. Ku, Z. An, B. Kalveram, A. N. Freiberg, V. D. Menachery, X. Xie, K. S. Plante, S. C. Weaver, P.-Y. Shi, Spike mutation D614G alters SARS-CoV-2 fitness. *Nature* **592**, 116–121 (2021). [doi:10.1038/s41586-020-2895-3](https://doi.org/10.1038/s41586-020-2895-3) [Medline](#)
7. K. H. D. Crawford, R. Eguia, A. S. Dingens, A. N. Loes, K. D. Malone, C. R. Wolf, H. Y. Chu, M. A. Tortorici, D. Veessler, M. Murphy, D. Pettie, N. P. King, A. B. Balazs, J. D. Bloom, Protocol and Reagents for Pseudotyping Lentiviral Particles with SARS-CoV-2 Spike Protein for Neutralization Assays. *Viruses* **12**, 513 (2020). [doi:10.3390/v12050513](https://doi.org/10.3390/v12050513) [Medline](#)
8. A. A. Latif, J. L. Mullen, M. Alkuzweny, G. Tsueng, M. Cano, E. Haag, J. Zhou, M. Zeller, E. Hufbauer, N. Matteson, C. Wu, K. G. Andersen, A. I. Su, K. Gangavarapu, L. D. Hughes;

the Center for Viral Systems Biology, Lineage comparison. outbreak.info (available at <https://outbreak.info/compare-lineages>), accessed 22 July 2021.

9. W. Zeng, G. Liu, H. Ma, D. Zhao, Y. Yang, M. Liu, A. Mohammed, C. Zhao, Y. Yang, J. Xie, C. Ding, X. Ma, J. Weng, Y. Gao, H. He, T. Jin, Biochemical characterization of SARS-CoV-2 nucleocapsid protein. *Biochem. Biophys. Res. Commun.* **527**, 618–623 (2020). [doi:10.1016/j.bbrc.2020.04.136](https://doi.org/10.1016/j.bbrc.2020.04.136) [Medline](#)
10. J. Cubuk, J. J. Alston, J. J. Incicco, S. Singh, M. D. Stuchell-Breterton, M. D. Ward, M. I. Zimmerman, N. Vithani, D. Griffith, J. A. Wagoner, G. R. Bowman, K. B. Hall, A. Soranno, A. S. Holehouse, The SARS-CoV-2 nucleocapsid protein is dynamic, disordered, and phase separates with RNA. *Nat. Commun.* **12**, 1936 (2021). [doi:10.1038/s41467-021-21953-3](https://doi.org/10.1038/s41467-021-21953-3) [Medline](#)
11. T. M. Perdikari, A. C. Murthy, V. H. Ryan, S. Watters, M. T. Naik, N. L. Fawzi, SARS-CoV-2 nucleocapsid protein phase-separates with RNA and with human hnRNPs. *EMBO J.* **39**, e106478 (2020). [doi:10.15252/embj.2020106478](https://doi.org/10.15252/embj.2020106478) [Medline](#)
12. C. B. Plescia, E. A. David, D. Patra, R. Sengupta, S. Amiar, Y. Su, R. V. Stahelin, SARS-CoV-2 viral budding and entry can be modeled using BSL-2 level virus-like particles. *J. Biol. Chem.* **296**, 100103 (2021). [doi:10.1074/jbc.RA120.016148](https://doi.org/10.1074/jbc.RA120.016148) [Medline](#)
13. H. Swann, A. Sharma, B. Preece, A. Peterson, C. Eldredge, D. M. Belnap, M. Vershinin, S. Saffarian, Minimal system for assembly of SARS-CoV-2 virus like particles. *Sci. Rep.* **10**, 21877 (2020). [doi:10.1038/s41598-020-78656-w](https://doi.org/10.1038/s41598-020-78656-w) [Medline](#)
14. J. Lu, G. Lu, S. Tan, J. Xia, H. Xiong, X. Yu, Q. Qi, X. Yu, L. Li, H. Yu, N. Xia, T. Zhang, Y. Xu, J. Lin, A COVID-19 mRNA vaccine encoding SARS-CoV-2 virus-like particles induces a strong antiviral-like immune response in mice. *Cell Res.* **30**, 936–939 (2020). [doi:10.1038/s41422-020-00392-7](https://doi.org/10.1038/s41422-020-00392-7) [Medline](#)
15. Y. L. Siu, K. T. Teoh, J. Lo, C. M. Chan, F. Kien, N. Escriou, S. W. Tsao, J. M. Nicholls, R. Altmeyer, J. S. M. Peiris, R. Bruzzone, B. Nal, The M, E, and N structural proteins of the severe acute respiratory syndrome coronavirus are required for efficient assembly, trafficking, and release of virus-like particles. *J. Virol.* **82**, 11318–11330 (2008). [doi:10.1128/JVI.01052-08](https://doi.org/10.1128/JVI.01052-08) [Medline](#)
16. P.-K. Hsieh, S. C. Chang, C.-C. Huang, T.-T. Lee, C.-W. Hsiao, Y.-H. Kou, I.-Y. Chen, C.-K. Chang, T.-H. Huang, M.-F. Chang, Assembly of severe acute respiratory syndrome coronavirus RNA packaging signal into virus-like particles is nucleocapsid dependent. *J. Virol.* **79**, 13848–13855 (2005). [doi:10.1128/JVI.79.22.13848-13855.2005](https://doi.org/10.1128/JVI.79.22.13848-13855.2005) [Medline](#)
17. S. Dent, B. W. Neuman, Purification of coronavirus virions for Cryo-EM and proteomic analysis. *Coronaviruses* **1282**, 99–108 (2015). [doi:10.1007/978-1-4939-2438-7_10](https://doi.org/10.1007/978-1-4939-2438-7_10) [Medline](#)
18. X. Lu, Y. Chen, B. Bai, H. Hu, L. Tao, J. Yang, J. Chen, Z. Chen, Z. Hu, H. Wang, Immune responses against severe acute respiratory syndrome coronavirus induced by virus-like particles in mice. *Immunology* **122**, 496–502 (2007). [doi:10.1111/j.1365-2567.2007.02676.x](https://doi.org/10.1111/j.1365-2567.2007.02676.x) [Medline](#)
19. L. Kuo, P. S. Masters, Functional analysis of the murine coronavirus genomic RNA packaging signal. *J. Virol.* **87**, 5182–5192 (2013). [doi:10.1128/JVI.00100-13](https://doi.org/10.1128/JVI.00100-13) [Medline](#)

20. K. Woo, M. Joo, K. Narayanan, K. H. Kim, S. Makino, Murine coronavirus packaging signal confers packaging to nonviral RNA. *J. Virol.* **71**, 824–827 (1997). [doi:10.1128/jvi.71.1.824-827.1997](https://doi.org/10.1128/jvi.71.1.824-827.1997) [Medline](#)
21. J. A. Fosmire, K. Hwang, S. Makino, Identification and characterization of a coronavirus packaging signal. *J. Virol.* **66**, 3522–3530 (1992). [doi:10.1128/jvi.66.6.3522-3530.1992](https://doi.org/10.1128/jvi.66.6.3522-3530.1992) [Medline](#)
22. A. Kanakan, N. Mishra, J. Srinivasa Vasudevan, S. Sahni, A. Khan, S. Sharma, R. Pandey, Threading the Pieces Together: Integrative Perspective on SARS-CoV-2. *Pathogens* **9**, 912 (2020). [doi:10.3390/pathogens9110912](https://doi.org/10.3390/pathogens9110912) [Medline](#)
23. T. Giroglou, J. Cinatl Jr., H. Rabenau, C. Drosten, H. Schwalbe, H. W. Doerr, D. von Laer, Retroviral vectors pseudotyped with severe acute respiratory syndrome coronavirus S protein. *J. Virol.* **78**, 9007–9015 (2004). [doi:10.1128/JVI.78.17.9007-9015.2004](https://doi.org/10.1128/JVI.78.17.9007-9015.2004) [Medline](#)
24. M. Ujike, C. Huang, K. Shirato, S. Makino, F. Taguchi, The contribution of the cytoplasmic retrieval signal of severe acute respiratory syndrome coronavirus to intracellular accumulation of S proteins and incorporation of S protein into virus-like particles. *J. Gen. Virol.* **97**, 1853–1864 (2016). [doi:10.1099/jgv.0.000494](https://doi.org/10.1099/jgv.0.000494) [Medline](#)
25. X. Deng, M. A. Garcia-Knight, M. M. Khalid, V. Servellita, C. Wang, M. K. Morris, A. Sotomayor-González, D. R. Glasner, K. R. Reyes, A. S. Gliwa, N. P. Reddy, C. Sanchez San Martin, S. Federman, J. Cheng, J. Balcerak, J. Taylor, J. A. Streithorst, S. Miller, B. Sreekumar, P.-Y. Chen, U. Schulze-Gahmen, T. Y. Taha, J. M. Hayashi, C. R. Simoneau, G. R. Kumar, S. McMahon, P. V. Lidsky, Y. Xiao, P. Hemarajata, N. M. Green, A. Espinosa, C. Kath, M. Haw, J. Bell, J. K. Hacker, C. Hanson, D. A. Wadford, C. Anaya, D. Ferguson, P. A. Frankino, H. Shivram, L. F. Lareau, S. K. Wyman, M. Ott, R. Andino, C. Y. Chiu, Transmission, infectivity, and neutralization of a spike L452R SARS-CoV-2 variant. *Cell* **184**, 3426–3437.e8 (2021). [doi:10.1016/j.cell.2021.04.025](https://doi.org/10.1016/j.cell.2021.04.025) [Medline](#)
26. A. Kuzmina, Y. Khalaila, O. Voloshin, A. Keren-Naus, L. Boehm-Cohen, Y. Raviv, Y. Shemer-Avni, E. Rosenberg, R. Taube, SARS-CoV-2 spike variants exhibit differential infectivity and neutralization resistance to convalescent or post-vaccination sera. *Cell Host Microbe* **29**, 522–528.e2 (2021). [doi:10.1016/j.chom.2021.03.008](https://doi.org/10.1016/j.chom.2021.03.008) [Medline](#)
27. Y. Liu, J. Liu, K. S. Plante, J. A. Plante, X. Xie, X. Zhang, Z. Ku, Z. An, D. Scharon, C. Schindewolf, V. D. Menachery, P.-Y. Shi, S. C. Weaver, The N501Y spike substitution enhances SARS-CoV-2 transmission. bioRxiv (2021), [doi:10.1101/2021.03.08.434499](https://doi.org/10.1101/2021.03.08.434499).
28. C. Motozono, M. Toyoda, J. Zahradnik, A. Saito, H. Nasser, T. S. Tan, I. Ngare, I. Kimura, K. Uriu, Y. Kosugi, Y. Yue, R. Shimizu, J. Ito, S. Torii, A. Yonekawa, N. Shimono, Y. Nagasaki, R. Minami, T. Toya, N. Sekiya, T. Fukuhara, Y. Matsuura, G. Schreiber, T. Ikeda, S. Nakagawa, T. Ueno, K. Sato; Genotype to Phenotype Japan (G2P-Japan) Consortium, SARS-CoV-2 spike L452R variant evades cellular immunity and increases infectivity. *Cell Host Microbe* **29**, 1124–1136.e11 (2021). [doi:10.1016/j.chom.2021.06.006](https://doi.org/10.1016/j.chom.2021.06.006) [Medline](#)
29. R. Kalkeri, Z. Cai, S. Lin, J. Farmer, Y. V. Kuzmichev, F. Koide, SARS-CoV-2 Spike Pseudoviruses: A Useful Tool to Study Virus Entry and Address Emerging Neutralization Escape Phenotypes. *Microorganisms* **9**, 1744 (2021). [doi:10.3390/microorganisms9081744](https://doi.org/10.3390/microorganisms9081744) [Medline](#)

30. Y. Weisblum, F. Schmidt, F. Zhang, J. DaSilva, D. Poston, J. C. Lorenzi, F. Muecksch, M. Rutkowska, H.-H. Hoffmann, E. Michailidis, C. Gaebler, M. Agudelo, A. Cho, Z. Wang, A. Gazumyan, M. Cipolla, L. Luchsinger, C. D. Hillyer, M. Caskey, D. F. Robbiani, C. M. Rice, M. C. Nussenzweig, T. Hatziioannou, P. D. Bieniasz, Escape from neutralizing antibodies by SARS-CoV-2 spike protein variants. *eLife* **9**, e61312 (2020). [doi:10.7554/eLife.61312](https://doi.org/10.7554/eLife.61312) [Medline](#)
31. W. T. Harvey, A. M. Carabelli, B. Jackson, R. K. Gupta, E. C. Thomson, E. M. Harrison, C. Ludden, R. Reeve, A. Rambaut, S. J. Peacock, D. L. Robertson; COVID-19 Genomics UK (COG-UK) Consortium, SARS-CoV-2 variants, spike mutations and immune escape. *Nat. Rev. Microbiol.* **19**, 409–424 (2021). [doi:10.1038/s41579-021-00573-0](https://doi.org/10.1038/s41579-021-00573-0) [Medline](#)
32. X. Ju, Y. Zhu, Y. Wang, J. Li, J. Zhang, M. Gong, W. Ren, S. Li, J. Zhong, L. Zhang, Q. C. Zhang, R. Zhang, Q. Ding, A novel cell culture system modeling the SARS-CoV-2 life cycle. *PLOS Pathog.* **17**, e1009439 (2021). [doi:10.1371/journal.ppat.1009439](https://doi.org/10.1371/journal.ppat.1009439) [Medline](#)
33. C. R. Carlson, J. B. Asfaha, C. M. Ghent, C. J. Howard, N. Hartooni, M. Safari, A. D. Frankel, D. O. Morgan, Phosphoregulation of Phase Separation by the SARS-CoV-2 N Protein Suggests a Biophysical Basis for its Dual Functions. *Mol. Cell* **80**, 1092–1103.e4 (2020). [doi:10.1016/j.molcel.2020.11.025](https://doi.org/10.1016/j.molcel.2020.11.025) [Medline](#)
34. S. Lu, Q. Ye, D. Singh, Y. Cao, J. K. Diedrich, J. R. Yates 3rd, E. Villa, D. W. Cleveland, K. D. Corbett, The SARS-CoV-2 nucleocapsid phosphoprotein forms mutually exclusive condensates with RNA and the membrane-associated M protein. *Nat. Commun.* **12**, 502 (2021). [Medline](#)
35. B. Li, A. Deng, K. Li, Y. Hu, Z. Li, Q. Xiong, Z. Liu, Q. Guo, L. Zou, H. Zhang, M. Zhang, F. Ouyang, J. Su, W. Su, J. Xu, H. Lin, J. Sun, J. Peng, H. Jiang, P. Zhou, T. Hu, M. Luo, Y. Zhang, H. Zheng, J. Xiao, T. Liu, R. Che, H. Zeng, Z. Zheng, Y. Huang, J. Yu, L. Yi, J. Wu, J. Chen, H. Zhong, X. Deng, M. Kang, O. G. Pybus, M. Hall, K. A. Lythgoe, Y. Li, J. Yuan, J. He, J. Lu, Viral infection and Transmission in a large well-traced outbreak caused by the Delta SARS-CoV-2 variant, medRxiv (2021); [doi:10.1101/2021.07.07.21260122](https://doi.org/10.1101/2021.07.07.21260122).